EAST HARTFORD, CONNECTICUT

H910092-12

Theoretical Investigation of the Radiant Emission Spectrum from the Fuel Region of a Nuclear Light Bulb Engine

NASA Contract No. NASw-847

UNITED AIRCRAFT CORPORATION

United Aircraft Research Laboratories

EAST HARTFORD, CONNECTICUT

United Aircraft Research Laboratories

UNITED AIRCRAFT CORPORATION

EAST HARTFORD, CONNECTICUT

H910092-12

Theoretical Investigation of the Radiant Emission Spectrum from the Fuel Region of a Nuclear Light Bulb Engine

NASA Contract No. NASw-847

REPORTED BY N. L. Krascella
N. L. Krascella

APPROVED BY W. G. Burwell
W. G. Burwell, Chief
Kinetics and Thermal
Sciences

DATE October 1969

NO. OF PAGES 50

COPY NO. 66.1

FOREWORD

An exploratory experimental and theoretical investigation of gaseous nuclear rocket technology is being conducted by the United Aircraft Research Laboratories under Contract NASw-847 with the joint AEC-NASA Space Nuclear Propulsion Office. The Technical Supervisor of the Contract for NASA is Captain C. E. Franklin (USAF). Results of portions of the investigation conducted during the period between September 15, 1968 and September 15, 1969 are described in the following five reports (including the present report) which comprise the required ninth Interim Summary Technical Report under the Contract:

1. Roman, W. C., J. F. Klein, and P. G. Vogt: Experimental Investigations to Simulate the Thermal Environment, Transparent Walls and Propellant Heating in a Nuclear Light Bulb Engine. United Aircraft Research Laboratories Report H-910091-19, September 1969.

2. Mensing, A. E. and J. F. Jaminet: Experimental Investigations of Heavy-Gas Containment in R-F Heated and Unheated Two-Component Vortexes. United Aircraft Research Laboratories Report H-910091-20, September 1969.

3. Krascella, N. L.: Theoretical Investigation of the Radiant Emission Spectrum from the Fuel Region of a Nuclear Light Bulb Engine. United Aircraft Research Laboratories Report H-910092-12, September 1969. (present report)

4. Latham, T. S., H. E. Bauer, and R. J. Rodgers: Studies of Nuclear Light Bulb Start-up Conditions and Engine Dynamics. United Aircraft Research Laboratories Report H-910375-4, September 1969.

5. Johnson, B. V.: Exploratory Experimental Study of the Effects of Inlet Conditions on the Flow and Containment Characteristics of Coaxial Flows. United Aircraft Research Laboratories Report H-910091-21, September 1969.

Report H910092-12

Theoretical Investigation of the Radiant Emission Spectrum from the Fuel Region of a Nuclear Light Bulb Engine

TABLE OF CONTENTS

Report H910092-12

Theoretical Investigation of the Radiant Emission Spectrum from the Fuel Region of a Nuclear Light Bulb Engine

SUMMARY

A theoretical investigation was conducted to determine the spectral emission characteristics of the fuel region of a nuclear light bulb engine and hence, the spectral radiative flux incident upon the transparent containment walls or upon the reflective end walls of such an engine. The analysis was performed for a specified engine configuration and for a specific nuclear fuel partial pressure distribution. Estimates of the spectral radiative flux emanating from the nuclear fuel region were made for a total radiated flux of 24,300 Btu/ft^2-sec (2.757×10^{11} erg/cm^2-sec), which corresponds to an effective black-body radiating temperature of 15,000°R (8333°K).

Six cases were considered in which the effects of changes in the heavy-atom absorption coefficient model parameters, the addition of a seeding gas, and changes in end-wall reflectivities on the spectral radiative flux emitted from the nuclear fuel region were examined. Three cases involved parametric variations of the heavy-atom model in either the fuel species ionization potentials or in the oscillator strength distribution functions describing line transitions. In the fourth case, the effect of hydrogen as a seed gas on the emitted spectral radiative flux was studied. The effect on the emitted flux of a uniform end-wall spectral reflectivity of 0.5 was examined in the fifth case; similar calculations were made in the sixth case using the spectral reflectivity of aluminum.

CONCLUSIONS

1. The spectral distribution of radiative flux emitted from the nuclear fuel region of a nuclear light bulb engine differs appreciably from that of a black body at a temperature of 15,000°R (8,333°K). If no seeds are employed, the spectral distribution from the fuel region is shifted to higher wave numbers (shorter wavelengths).

2. Addition of a seed gas such as hydrogen tends to attenuate the radiation emitted in the ultraviolet region of the spectrum.

3. Use of end walls with reflective coatings such as aluminum tends to shift the spectral distribution of radiated energy to higher wave numbers (shorter wavelengths) for a given total flux emitted from the fuel.

4. The radiation spectrum emitted from the fuel region is controlled by a very thin layer of fuel near the edge of the fuel region because of the highly opaque nature of nuclear fuel.

INTRODUCTION

Analytical and experimental investigations of various aspects of gaseous nuclear rocket technology are currently being conducted by the Research Laboratories of United Aircraft Corporation under Contract NASw-847 administered by the joint AEC-NASA Space Nuclear Propulsion Office. Of primary interest under this contract is the nuclear light bulb engine concept described in Ref. 1. In this concept, a vortex-stabilized gaseous nuclear reactor emits thermal radiation which is utilized to heat a seeded hydrogen propellant. The nuclear fuel and seeded propellant regions are physically separated by an internally cooled transparent wall. Knowledge of the spectral distribution of thermal radiation emitted from the nuclear fuel region and subsequently incident upon the transparent containment wall is necessary in analyzing the feasibility of the nuclear light bulb engine concept.

To date most calculations of the flux of thermal radiation emitted from the nuclear fuel have assumed that the emitted radiation originates from a grey-gas at the assumed edge-of-fuel temperature (Refs. 2 and 3). Preliminary calculations indicate that the spectral distribution of thermal radiation differs appreciably from that of a black body. However, the effect of changes in the heavy-atom model parameters (used to describe the composition and spectral properties of the nuclear fuel) on the emitted spectral flux have not been assessed; similarly, the effect of the addition of seed gases on the emitted flux have not been studied.

An additional problem arises in considering radiation emitted from the fuel region in an axial direction. Axially directed radiation impinges upon highly reflecting end walls in the full-scale engine. It is anticipated that a large fraction of the incident flux will be reflected. Obviously a large flux of reflected radiation will significantly alter the edge-of-fuel temperature in an axial direction as well as the temperature distribution in the outer layer of fuel adjacent to the reflecting wall. No estimates of the effect of highly reflecting end walls on the spectral distribution of radiant flux emitted from the fuel region have been made to date.

Based on the preceeding discussion, a program was formulated to determine the effect on the spectral radiation emitted from the fuel region of a nuclear light bulb engine of: (a) changes in the heavy-atom model parameters; (b) addition of a seed gas and (c) inclusion of reflective end walls. The program is described in detail in succeeding sections of this report.

ANALYTICAL METHOD

Because of the high fuel opacity, the radiation spectrum emitted from the fuel region of a nuclear light bulb engine is controlled by conditions existing in the outermost layer of the region. At the temperatures and pressures anticipated in the full-scale engine, the dominating region is typically a few centimeters in depth. Thus, the region controlling spectral radiation emission may be considered as a plane-parallel gas layer containing a relatively low concentration of nuclear fuel. Since low nuclear fuel density in the edge-of-fuel region precludes extensive energy release by nuclear fission in this region, the outermost layer of fuel is characterized by a constant total energy flux at all points within the region.

The spectral distribution of emitted flux may be estimated using a transport analysis of the radiative transfer process. The radiation flux profile is a function of the temperature distribution in the outer fuel layer as well as the composition and spectral absorption coefficients of the nuclear fuel. These fuel properties are functions of both pressure and temperature.

Iterative Procedure

The temperature and corresponding radiative flux profile may be determined for a specified fuel concentration profile utilizing existing one-dimensional UARL simplified grey-gas and spectral transport computer codes.

1. To initiate the procedure, a distribution of Rosseland Mean Opacity as a function of temperature is assumed for a specified fuel partial pressure variation with position in the fuel region. These mean opacity data, a specified total heat flux, Q^*, (constant throughout the medium) and an edge-of-fuel temperature are used as input for the simplified grey-gas computer code to calculate a temperature profile using the optically thick approximation.

2. The temperature profile estimated in Step 1 and a specified fuel partial pressure distribution are used as input for the spectral transport computer code to calculate the corresponding fuel absorption coefficients and the spectral flux distribution at each position within the outer layer of the fuel. Finally, the spectral fluxes at each position are integrated to ascertain the total flux, Q_i.

3. The assumed Rosseland Mean Opacities used in Step 1 are modified by the relationship:

$$a_{R_{i+1}} = a_{R_i}\left(\frac{Q_i}{Q^*}\right) \qquad (1)$$

where a_{R_i}, $a_{R_{i+1}}$, are values of the Rosseland Mean Opacity for the initial and second iterations respectively, Q_i is the total flux (integrated spectral flux) calculated in Step 2, and Q* is the desired total and constant flux radiated from the fuel region.

4. Step 1 is repeated using $a_{R_{i+1}}$ values, and the same sequence is repeated until Q_i and Q* agree to within 5% at all radial positions in the fuel region. (Approximately 10 iterations are normally required to achieve convergence).

The edge-of-fuel temperature required to initiate the calculation is determined by application of the "temperature jump approximation" as described in Ref. 4. Assuming no back radiation is incident upon the fuel region from the containing wall and assuming that the fuel region can be represented as a grey gas, the edge-of-fuel temperature is approximated by:

$$T_E = \left(\frac{Q^*}{2\sigma}\right)^{\frac{1}{4}} \tag{2}$$

where Q* is the assumed constant radiative flux in the outermost layer of fuel, and σ is the Stefan-Bolzmann constant. If the containing wall is reflective and can be represented as a grey surface, Eq. (2) is modified by the grey-surface reflectivity and is given by:

$$T_E = \left(\frac{Q^*}{2(1-\langle r\rangle)\sigma}\right)^{\frac{1}{4}} \tag{3}$$

where $\langle r\rangle$ is the grey-surface reflectivity of the wall material. It is shown in the following sections that Eqs. (2) and (3) are not valid for non-grey-gas conditions.

Unit Cavity Configuration and Conditions

A fuel-containment region 0.681 ft (20.75 cm) in radius at a total pressure of 500 atm was selected for the radiation emission analysis of the nuclear light bulb engine unit cavity schematically depicted in Fig. 1. It was assumed that nuclear fuel existed at a constant pressure of 200 atm from the centerline or core of the containment region out to a radius of 0.3405 ft (10.38 cm). At radial positions beyond 0.3405 ft, the fuel partial pressure decreased linearly to a pressure of 0.01 atm at the edge-of-fuel position. The fuel partial pressure profile is graphically illustrated in Fig. 2. Note that the distance, y, in the fuel region is measured from the edge-of-fuel position (y=0) inward to the centerline (y=20.75 cm) for analysis of the spectrum emitted radially outward (cases 1 through 4, see following section). For analysis of the spectrum emitted in an axial direction, y, is measured in the axial direction (cases 5 and 6, see following section). The

difference between the total pressure of 500 atm and the fuel partial pressure at any position was attributed to neon (the absorption of the neon was neglected).

All calculations were made for an assumed effective radiating temperature, T*, of 15,000°R (8333°K) which corresponds to an effective total radiative black-body flux Q* of 24,300 Btu/ft^2-sec (2.757 x 10^{11} erg/cm^2-sec). This effective total flux was taken as a constant at the outer fuel positions considered as a consequence of the assumption of negligible energy generation by the fuel in this region.

Spectral quantities were calculated for at least twenty-five wave numbers between 1.0 x 10^3 (10.0μ) and 1.0 x 10^6 cm^{-1} (0.01μ). Edge-of-fuel temperatures required to initiate the iterative procedure were calculated by means of Eq. (2) for cases 1 through 4 and by means of Eq. (3) for cases 5 and 6. Edge-of-fuel temperatures calculated by the iterative pores for cases 1 through 4 was 10,650°R (5,917°K), for case 5, 14,650°R (8,139°K), and for case 6, 19,650°R (10,917°K).

Description of Cases

The analytical scheme, cavity configuration and conditions described in preceding paragraphs were employed in all subsequent calculations of the spectral distributions of radiative energy emanating from the nuclear fuel region of a nuclear light bulb engine. The six cases examined during the investigation considered the effects on the spectral distribution of radiation of (a) variations in the parameters depicting the heavy-atom model which was used to estimate the composition and spectral absorption characteristics of the fuel ionization species (b) addition of a seed gas, hydrogen, to the system and (c) the inclusion of reflective end walls.

The heavy-atom model(Refs. 5 and 6) was required in order to calculate the requisite composition and spectral absorption characteristics of the nuclear fuel as a function of temperature and pressure for use as input in the spectral transport machine code. In cases 1 and 2 the continuum-type oscillator distribution function was employed to define transition probabilities in the line region of the fuel spectrum. With the continuum approximation, distinct line structure in heavy-atom spectra is ignored and the absorption coefficients are slowly varying functions of wave number (see Refs. 5 and 6 for details). Cases 1 and 2 differ in the fuel species ionization potentials employed. The ionization potentials for case 1 are termed the low set and were of the following magnitude: 6.1, 11.46, 17.94 and 31.14 ev (Ref. 7); similar ionization potential data for case 2 are termed the high set and were of the following magnitude: 6.1, 17.1, 38.8 and 65.6 ev (Ref. 8).

In case 3, the low ionization potentials of case 1 were retained; however a band type oscillator strength distribution function was used in the heavy-atom model.

In the band type oscillator strength distribution function, transition probabilities in the line region are approximated by summing known oscillator strengths for various lines in the fuel spectrum over wavelength intervals of 200 Å. The method is described in Ref. 9 and is an approximation designed to account for line structure in the fuel spectrum. Typical oscillator strength data (Refs. 10 and 11) for neutral and singly ionized uranium summed over wavelength intervals of 200 Å are shown in Fig. 3. Similar data for doubly and triply ionized uranium are not available in the current literature; therefore the distribution for singly ionized uranium given in Fig. 3 was used in the heavy-atom model for the higher ionization species.

The effects of seed gas on the emitted flux was examined in case 4 in which the heavy-atom model parameters of case 1 were retained. Hydrogen was selected as a seed gas and introduced at a uniform pressure of 10 atm at all radial positions in the fuel-containment region.

Cases 5 and 6 represent a study of end-wall effects in which a fraction of the energy emitted from the fuel region in an axial direction could be reflected back into the fuel. In both cases the heavy-atom model parameters of case 1 were incorporated. In case 5 a uniform end-wall reflectivity of 0.50 was assumed at all wavelengths as shown in Fig. 4 by the horizontal dashed line. In case 6, the end walls were considered to be aluminum and the spectral reflectivity of aluminum (Refs. 12 through 15) was used in the system. This spectral reflectivity profile is also graphically illustrated in Fig. 4.

The various conditions and approximations used in cases 1 through 6 are summarized in Table I for reference.

SPECTRAL EMISSION FROM THE
NUCLEAR FUEL REGION

Temperature Distributions

Approximately ten iterations were required in each case in order to achieve convergence between the simplified grey-gas code and the spectral transport code. A calculation was considered as complete in any case investigated when the total flux at all radial positions computed by means of the spectral transport code (using the temperature profile estimated by means of the simplified grey-gas code) agreed with the effective black-body flux of 24,300 Btu/ft^2-sec to within 5%. Note that case 6 represents an exception to the 5% criterion. The iterative procedure was terminated after 10 iterations for case 6 with a tolerance of approximately 10% for the first few positions near the fuel edge. The total flux at each radial position calculated using the spectral transport code is obtained by integration of the spectral flux at each radial position. Total flux distributions which are indicative of convergence are illustrated in Fig. 5 for each of the cases studied. It should be noted that the excellent results exhibited in Fig. 5 were obtained by reducing the predicted edge-of-fuel temperature (see Eq. (2)) in cases 1 through 4 by approximately 15%. The edge-of-fuel temperature predicted by Eq. (3) for case 5 involving a uniform wall reflectivity was decreased approximately 2% in order to obtain the total flux distributions illustrated in Fig. 5. Equation (3) was not used to estimate the edge-of-fuel temperature for case 6 because of the marked spectral dependence of the aluminum reflectivity. The edge-of-fuel temperature for this case was determined by means of the iterative procedure previously described.

Final temperature distributions as a function of the distance from the fuel edge for all cases examined are graphically compared in Fig. 6. Cases 1, 2 and 3 demonstrate the effect of changes in the heavy-atom model parameters on the temperature distribution. Increasing the magnitude of the fuel species ionization potentials tends to increase the temperature at any position in the outer fuel region as is shown in Fig. 6 by the curves for case 1 (low ionization potentials) and case 2 (high ionization potentials). A comparison of curves 1 and 3 shows that using the band type oscillator strength distribution in the heavy-atom model (case 3) results in a less severe temperature gradient than that predicted on the basis of a heavy-atom model with a continuous oscillator strength distribution (case 1).

Comparing curves for cases 3 and 4 in Fig. 6 shows the effect on the temperature distribution of the addition of 10 atm of hydrogen as a seeding gas. The same heavy-atom model parameters were used for both cases. The presence of hydrogen tends to increase the temperature gradient at any position within the outer layer of the fuel region.

The curves in Fig. 6 for cases 5 and 6 exhibit the anticipated increase in edge-of-fuel temperature as a result of reflection of radiation from the end walls.

Spectral Absorption Coefficients at Edge-of-Fuel Conditions

Typical spectral absorption coefficients for edge-of-fuel conditions are compared in Fig. 7 for cases 1, 2 and 3, in Fig. 8 for cases 3 and 4, and in Fig. 9 for cases 1,5 and 6. These data and similar data for conditions at various positions within the fuel are required as input to the spectral transport code.

Comparison of the curves in Fig. 7 for cases 1, 2 and 3 show the effect of changes in the ionization potentials and oscillator strength distribution functions used to describe the heavy-atom model. The curves for cases 1 and 2 show the effect of variations in fuel species ionization potentials. Incorporation of the low set of ionization potential data in the heavy-atom model for case 1 results in higher values of the absorption coefficients than those of case 2 for wave numbers up to approximately 40,000 cm^{-1}. At wave numbers greater than 40,000 cm^{-1}, the low set of ionization potentials result in absorption coefficients which are lower than those calculated for the heavy-atom model using the high set of ionization potentials. A comparison of curves for cases 1 and 2 with the curve for case 3 illustrates typical results obtained for the spectral absorption coefficients by replacing the continuous oscillator strength distribution function of cases 1 and 2 with the band type oscillator strength distribution function used in case 3. (Note that the low set ionization potentials were used for cases 1 and 3). A band type oscillator strength distribution function (case 4) results in a stronger wave number dependence of the absorption coefficient than does the continuous oscillator strength distribution function used in cases 1 and 2. In addition, the band type distribution (case 3) results in an absorption coefficient distribution which is much lower in magnitude than that predicted for the continuous oscillator strength distribution (cases 1 and 2) at wave numbers less than approximately 25,000 cm^{-1}.

In Fig. 8 a comparison is made between case 3 (no hydrogen seed gas) and case 4 (10 atm of hydrogen seed gas). Since the same heavy-atom model was used in cases 3 and 4, the dashed curve in Fig. 8 illustrates the fuel spectral absorption coefficient distribution with wave number for both cases at the edge-of-fuel conditions. The solid curve (case 4) represents the calculated spectral absorption coefficient of 10 atm of hydrogen at the edge-of-fuel temperature of 10,650°R. The sharp peak in the solid curve at a wave number of approximately 82,000 cm^{-1} is due to the Lyman- α line of atomic hydrogen. The pronounced edge in the solid curve at a wave number of approximately 105,000 cm^{-1} represents the threshold for absorption from the Lyman bound-free continuum of atomic hydrogen.

Similar comparisons in the spectral absorption coefficient distributions at the edge-of-fuel conditions are graphically depicted in Fig. 9 for cases 1, 5 and 6 which differ with respect to the reflectivity of the end walls. In case 1, which is used as a standard of comparison, reflective end walls were omitted; in case 5, an end wall with uniform reflectivity was considered; in case 6, an end wall of aluminum was treated. A comparison of the curves for cases 1, 5 and 6 in Fig. 9 shows that the general contour for each absorption coefficient distribution is approximately the same. This result is expected since the same heavy-atom model configuration was used in all cases. The lower values of the absorption coefficient for case 5, as contrasted with those for case 1, reflect the decreased fuel density at the edge of the fuel in case 5. The fuel pressure was 0.01 atm for all cases; however, the edge-of-fuel temperature for case 5 was 14,650°R as compared to 10,650°R for case 1. Similar reasoning applies when the absorption coefficient results of case 6 and case 1 are compared. Note that the edge-of-fuel temperature for case 6 was 19,650°R.

The same combinations of cases will be used in all subsequent figures and discussions to enable comparison of results for changes in heavy-atom model parameters (cases 1, 2 and 3), effect of seeding gases (cases 3 and 4) and effect of wall reflectivities (cases 1, 5 and 6).

Density Profiles

The composition data required to compute the spectral absorption coefficient results previously discussed were used to estimate nuclear fuel and total density profiles as a function of position within the outer layer of the fuel region.

Fuel Density

Nuclear fuel density distributions for each of the cases examined are compared in Fig. 10 for cases 1, 2 and 3, in Fig. 11 for cases 3 and 4, and in Fig. 12 for cases 1, 5 and 6. The fuel density distributions for all cases exhibit similar behavior and are of the same magnitude at any specified position within the outer layer of the fuel region. The density at the edge-of-fuel conditions for cases 1, 2 and 3 (temperature of 10,650°R and fuel pressure of 0.01 atm) was 1.78×10^{-4} lb/ft^3. For cases 5 and 6 the edge-of-fuel temperatures were higher, 14,650°R for case 5 and 19,650°R for case 6. The densities for these cases were correspondingly lower, 1.09×10^{-4} lb/ft^3 for case 5 and 5.81×10^{-5} lb/ft^3 for case 6.

Total Density

The total density is defined as the sum of the densities of all gas species present in the system. For case 1, 2, 3, 5 and 6 the gases present in the system examined were nuclear fuel and neon. For case 4, 10 atm of hydrogen was added to the fuel-neon system as a seeding gas. Total density is plotted as a function of position in Fig. 13 for cases, 1, 2 and 3, in Fig. 14 for cases 3 and 4, and in Fig. 15 for cases 1, 5 and 6.

Spectral Radiative Energy Profiles

Spectral distributions of radiative flux emitted from the nuclear fuel region of a typical nuclear light bulb rocket engine are graphically depicted in Figs. 16, 18 and 20 for all cases investigated. In Figs. 17, 19 and 21 the results of the spectral distributions illustrated in Figs. 16, 18 and 20 are replotted as relative fractional flux distributions. These curves given the relative fraction of total energy radiated between wave numbers of 1.0×10^3 cm^{-1} and any specified wave number ω and between any wave number ω and a wave number of 1.0×10^6 cm^{-1}. Also shown for comparison purposes in Figs. 16 through 21 are the spectral and relative fractional flux distributions for a black body at temperatures of 10,000°R (5,556°K), 15,000°R (8,333°K) and 20,000°R (11,111°K). As noted previously, all estimates of spectral radiative flux emitted from the nuclear fuel were made for a constant total flux of 24,300 Btu/ft^2-sec (2.757×10^{11} erg/cm^2-sec) corresponding to an effective black-body radiating temperature of 15,000°R (8,333°K).

Effect of Changes in Heavy-Atom Model Parameters

In Fig. 16 the effect of variations in the heavy-atom model parameters on the spectral flux emitted from the fuel region are illustrated. In cases 1 and 2, using the continuum oscillator strength distribution function in the heavy-atom model and different ionization potentials, only moderate differences in the spectral energy distribution curves are noted as shown in Fig. 16. In both cases (cases 1 and 2) the spectral flux was less than that of a black body at a temperature of 15,000°R for wave numbers between 1.0×10^3 and approximately 2.5×10^4 cm^{-1} (wavelengths between 10.0 and 0.4 μ). For wave numbers greater than approximately 2.5×10^4 cm^{-1} (wavelengths less than 0.4 μ), cases 1 and 2 resulted in spectral flux distributions which were lower than that of a 15,000°R black body. It should be noted that increasing the magnitudes of the ionization potentials used in the heavy-atom model (Case 1 used the low set, case 2 the high set) tended to shift the spectral flux distribution such that somewhat more energy was radiated at wave numbers greater than about 2.5×10^4 cm^{-1} (wavelengths less than 0.4 μ) in case 2 as compared to case 1.

In case 3, the low ionization potentials and a band type oscillator strength distribution function were used in the heavy-atom model. More drastic changes appear in the spectral flux distribution than those noted between cases 1 and 2. The spectral flux for case 3 exceeded that of a black body at a temperature of 15,000°R for wave numbers between 1.0×10^3 and 1.0×10^4 cm^{-1} (wavelengths between 10.0 and 1.0 μ). The smoothly varying spectral flux distribution observed for cases 1 and 2 was also noted for case 3 up to a wave number of 1.0×10^4 cm^{-1} (wavelength 1.0 μ). However, the spectral structure noted for the case 3 spectral absorption coefficient distribution (see Fig. 7) was reflected in the spectral flux distribution at wave numbers between 1.0×10^4 and 1.0×10^5 cm^{-1} (wavelengths between 1.0 and 0.1 μ). Two "windows" are observed at wave numbers of approximately 3.0×10^4 and 5.5×10^4 cm^{-1} (wavelengths at 0.33 and 0.182 μ). Similarly, two peaks in the spectral flux dis-

tributions are observed at wave numbers of 4.0×10^4 and 7.5×10^4 cm^{-1} (wavelengths at 0.25 and 0.133 μ). In general the spectral flux for case 3 was less than that for a 15,000°R black body between wave numbers of approximately 1.0×10^4 and 7.0×10^4 cm^{-1} (wavelengths at 1.0 and 1.143 μ). The peak at a wave number of 4.0×10^4 cm^{-1} (wavelength at 0.25 μ) was about equal to the 15,000°R black-body flux. For wave numbers greater than 5.5×10^4 cm^{-1} (wavelengths less than 0.33 μ) the emitted spectral flux exceeds that of a 15,000°R black body.

The spectral flux results of Fig. 16 for cases 1, 2 and 3 as well as the spectral flux results for a black body at the indicated temperatures (10,000, 15,000 and 20,000°R) were used to estimate relative fractional flux distributions. These data (relative fractional fluxes) are plotted as a function of wave number in Fig. 17 and give the fraction of the radiation emitted in any wave number interval relative to the total flux radiated over all wave numbers. The results illustrated in Fig. 17 show that considerably more energy is radiated in the visible and ultraviolet spectral regions by the nuclear fuel than a black body at a temperature of 15,000°R (8,333°K).

For example, the fraction of total energy radiated by a 15,000°R (8,333°K) black body in the wave numbers interval between 5×10^{-4} and infinity (wavelengths between 0.2 and 0 μ) is 2.5×10^{-2}, which is equivalent to a flux of 6.08×10^2 Btu/ft^2-sec. The relative fraction of emitted energy from the nuclear fuel is 3.6×10^{-1} (8.42×10^3 Btu/ft^2-sec) for case 1, 2.4×10^{-1} (5.62×10^3 Btu/ft^2-sec) for case 2 and 2.6×10^{-1} (6.08×10^3 Btu/ft^2-sec) for case 3. Similar results are obtained for other wave number intervals.

A number of trends are observed in Fig. 17 which reflect changes in the heavy-atom model parameters. In general, decreasing the ionization potentials used in the heavy-atom model tends to shift more energy toward the ultraviolet spectral region as is shown in Fig. 17 by comparing the results for case 1 (low ionization potentials) and case 2 (high ionization potentials). A comparison of the results for cases 1 and 3 shows that using the band type oscillator strength distribution function in the heavy-atom model(case 3) tends to shift the overall relative fractional flux distribution toward the infrared spectral region.

Effect of Seed Gas

The preceeding results indicated that a large fraction of the radiation emitted from the nuclear fuel region occurs at wave numbers where the transparent containment walls become effectively opaque. (Wave numbers greater than approximately 5.0×10^4 cm^{-1} or wavelengths less than 0.2 μ). Thus, the energy incident upon the containment wall radiated by a pure nuclear fuel system would prove to be a severe heating and cooling problem with respect to the containment wall. In recognition of the containment-wall cooling problem, the radiative properties of the seed-fuel gas system were estimated with 10 atm of hydrogen added to the fuel region as a seeding gas.

Results of the seed gas analysis (case 4) are presented in Fig. 18 (spectral flux as function of wave number) and in Fig. 19 (relative fractional flux as a function of wave number). Also shown for comparison in Figs. 18 and 19 are the results for a pure fuel system (case 3). As shown in Fig. 18, a notable difference between cases 3 and 4 occurs in the "window" at a wave number of approximately 5.5×10^4 cm^{-1} (wavelength 0.182 μ). The depth of the "window" increased by about an order of magnitude and was shifted to a higher wave number (6.2×10^4 cm^{-1} or a wavelength of 0.161 μ) as a result of adding hydrogen as a seed gas. In addition, the radiation emitted by the fuel in case 3 at wave numbers greater than 1.0×10^5 cm^{-1} (wavelengths less than 0.1 μ) was drastically reduced in case 4 due to the addition of hydrogen.

These results are shown in Fig. 19 for cases 3 and 4 as the relative fractional flux distribution. The curves in Fig. 19 illustrate the reduction in the relative fractional flux in the visible and ultraviolet spectral region upon addition of hydrogen gas as a seeding agent. The results also suggest that seeding with selective gases would undoubtedly further reduce the quantity of radiation emitted in the critical region at wave numbers beyond approximately 5×10^4 cm^{-1} (wavelengths less than 0.2 μ). Two promising seed materials are diatomic oxygen and water vapor, both of which are very opaque at wavelengths less than 0.2 (wave numbers greater than 50,000 cm^{-1}). The primary difficulty is that both of these molecules tend to dissociate at high temperatures, although preliminary calculations indicate that there will be a significant fraction of undissociated molecules at temperatures of interest. Even if these molecules should dissociate at high temperatures, however, they would provide a protective blanket between the fuel and the wall at lower temperatures to protect the wall from overheating due to absorption of ultraviolet radiations. Additional calculations of the effect of seed addition, including considerations of chemical reactions between the seeds and the nuclear fuel, should be considered in future programs.

Effect of Reflective Walls

In cases 5 and 6 the heavy-atom model configuration of case 1 was used to examine the effect of wall reflectivities on the spectral flux emitted from the fuel region. A uniform reflectivity of 0.5 was used for all wave numbers for case 5, while the spectral reflectivity of aluminum (see Fig. 4) was used for case 6.

Spectral flux distributions as a function of wave number are compared in Fig. 20 for cases 1, 5 and 6; relative fractional flux distribution as a function of wave number are compared in Fig. 21 for these cases. Examination of Figs. 20 and 21 shows that relatively little change in the spectral flux distribution or in the relative fractionl flux distribution occurred between case 1 and case 5 as a result of including an end wall with a uniform spectral reflectivity. However, a marked change in the spectral distribution for case 6 (aluminum spectral reflectivity)was evident. For a wave number of approximately 1.0×10^3 cm^{-1} (wavelength of 10.0 μ), the predicted

spectral flux for case 6 was an order of magnitude less than that predicted for case 1. At a wave number of 1.0×10^4 cm^{-1} (wavelength of 10.0 μ), the difference between the predicted fluxes for case 6 as compared to case 1 was a factor of approximately 5. For wave numbers between 1.0×10^4 cm^{-1} and 5.8×10^4 (wavelengths between 0.1 and 0.173 μ), the spectral flux distributions for these cases converge. At wave numbers greater than approximately 5.8×10^4 cm^{-1} (0.173 μ or less) the spectral flux for case 6 exceeded the spectral flux for case 1. A small peak was also introduced into the spectral distribution of case 6 at a wave number of 8.0×10^4 cm^{-1} (0.125 μ) as a result of the spectral reflectivity of aluminum.

Similar trends are observed in the relative fractional flux distributions shown in Fig. 21 for cases 1, 5 and 6. In general, including reflective walls tends to shift the distribution such that more of the emitted energy falls in the visible and ultraviolet spectral regions.

Optical Depths at Selected Wave Numbers

In order to ascertain the thickness of fuel which influences the spectral radiative flux at the edge of fuel, it is necessary to know the "effective" optical depth. The optical depth at any wave number is given by the following equation:

$$\tau_\omega = \int_0^y a_\omega \, dy \tag{4}$$

where y is the distance from the fuel edge and a is the spectral absorption coefficient as a function of y. Spectral absorption coefficient data such as those given in Figs. 7, 8 and 9 were used to compute the optical depths as a function of distance into the fuel for each of the cases investigated at wave numbers of 2.0×10^3 (5.0 μ), 1.0×10^4 (1.0 μ), 2.0×10^4 (0.5μ), 5.0×10^4 (0.2μ) and 1.0×10^5 cm^{-1} (0.1μ). These results are graphically illustrated in Figs. 22 through 27 for cases 1 through 6 respectively.

In practice, the spectral flux of radiative energy emitted from the fuel region is not appreciably influenced by conditions more than 2 to 3 optical depths into the interior of the fuel containment region as shown by the results of this section. For cases 1 and 2 (see Figs. 22 and 23) this optical depth is reached or exceeded for all wave numbers less than 1.0×10^5 cm^{-1} (0.1 μ) at a position within 0.5 cm of the fuel edge. At a wave number of 1.0×10^5 cm^{-1} (0.1 μ) the optical depth criterion was not met; however less than 10% of the radiation was emitted at wave numbers greater than 1.0×10^5 cm^{-1} (0.1μ)(see Fig. 17).

Use of the band type oscillator strength distribution functions in the heavy-atom model for cases 3 and 4 resulted in a marked reduction in the optical depth at a wave number of 2.0×10^3 cm^{-1} (5.0 μ) as indicated in Figs. 24 and 25. The spectral region about a wave number of 2.0×10^3 cm^{-1} (5.0 μ) was relatively unimportant in the

analysis of these cases since a negligible quantity of radiation was emitted in this spectral region (see Fig. 19). The addition of hydrogen as a seed gas (case 4) tended to decrease the optical depth at a wave number of 1.0×10^4 cm^{-1} ($1.0\ \mu$) compared to case 3 (no hydrogen seed). Similarly, addition of hydrogen to the fuel system resulted in an increase in the calculated optical depths at a wave number of 1.0×10^5 cm^{-1} ($0.1\ \mu$).

Equivalent optical depth results are presented in Fig. 26 for case 5 involving an end wall of uniform reflectivity and in Fig. 27 for case 6 which involves an end wall with aluminum reflectivity. The most notable change in optical depth occurred in case 6 for a wave number of 1.0×10^5 cm^{-1} ($0.1\ \mu$) (see Fig. 27).

Effective Spectral Black-Body Properties of the Fuel Region

In Fig. 28 black-body fluxes are illustrated as a function of temperature for selected wave numbers. These results were used to estimate the effective spectral black-body radiating temperature T_{bb}, of the nuclear fuel region as a function of wave number as graphically depicted in Fig. 29 for all six cases investigated. The effective spectral black-body radiating temperature is defined as that temperature for which the spectral flux emitted by the fuel region at wave number ω is equal to a black-body spectral flux at wave number ω.

A number of general trends are observed in the results presented in Fig. 29. For cases 1, 2 and 3, the fuel systems radiate at an equivalent black-body temperature less than 15,000°R (8,333°K) in the wave number region between 1.0×10^3 ($10.0\ \mu$) and approximately 4.0×10^4 cm^{-1} ($0.25\ \mu$). At a wave number of about 4.0×10^4 cm^{-1} ($0.25\ \mu$) the fuel systems radiate like a black body at a temperature of 15,000°R (8,333°K). Between wave numbers of 4.0×10^4 ($0.25\ \mu$) and 1.0×10^5 cm-1 ($0.1\ \mu$) the effective radiating temperature for cases 1, 2 and 5 rapidly increases. The maximum effective radiating temperature of about 22,500°R (12,500°K) occurs at a wave number of 1.0×10^5 cm^{-1} ($0.1\ \mu$) for these three cases. Note that an end wall of uniform reflectivity (case 5) tended to reduce somewhat the effective radiating temperature for wave numbers between 1.0×10^3 ($10.0\ \mu$) and 1.0×10^4 cm^{-1} ($1.0\ \mu$). Similarly, the results for case 6 show that inclusion of an end wall with aluminum reflectivity drastically reduces the effective black-body radiating temperature between wave numbers of 1.0×10^3 ($10.0\ \mu$) and approximately 2.0×10^4 cm^{-1} ($0.50\ \mu$) as compared to case 1.

Similar calculated data are shown in Fig. 29 for cases 3 and 4. These results exhibit a marked increase in effective radiating temperature in the low wave number region between 1.0×10^3 ($10.0\ \mu$) and approximately 1.0×10^4 cm^{-1} ($1.0\ \mu$). At wave numbers greater than 1.0×10^4 cm^{-1} ($1.0\ \mu$) the effective spectral black-body radiating temperatures for cases 3 and 4 are approximately equivalent to those for case 1, 2, 5 and 6 and exhibit the same general trends. A marked peak in the effective radiating temperature occurs in the distribution for case 4 at a wave number of approximately 4.0×10^4 cm^{-1} ($0.25\ \mu$).

Effective Optical Depths of the Fuel Region

In Fig. 30, the effective optical depth is plotted as a function of wave number. The effective optical depth is defined as that optical depth at which the effective spectral black-body temperature and the gas temperature are equal. It is a measure of the effective distance one can "see" into the plasma.

Note that only one point could be calculated for case 6. The value of the effective optical depth was 1.83 at a wave number of 1.0×10^5 cm^{-1} ($0.1\,\mu$). Similarly, data could not be calculated for case 5 at wave numbers less than 5.0×10^4 cm^{-1} ($0.2\,\mu$). These data were not available since the estimated spectral black-body temperatures (see Fig. 29) at the indicated wave numbers were less than the gas temperatures plotted in Fig. 6.

In the remaining data plotted in Fig. 30 a number of trends are evident. The effective optical depth tends to increase with increasing wave number (decreasing wavelength) for all cases examined. For cases 2, 3 and 4 the effective optical depth decreases with increasing wave number between 1.0×10^4 ($0.1\,\mu$) and 2.0×10^4 cm^{-1} ($0.5\,\mu$).

REFERENCES

1. McLafferty, G. H. and H. E. Bauer: Studies of Specific Nuclear Light Bulb and Open-Cycle Vortex-Stabilized Gaseous Nuclear Rocket Engines. UARL Report F-910093-7, September 1967. Also issued as NASA CR-1030, 1968.

2. Kesten, A. S. and R. B. Kinney: Theoretical Effect of Changes in Constituent Opacities on Radiant Heat Transfer in a Vortex-Stabilized Gaseous Nuclear Rocket. UARL Report D-910092-5, September 1965.

3 Kesten, A. S. and N. L. Krascella: Theoretical Investigation of Radiant Heat Transfer in the Fuel Region of a Gaseous Nuclear Rocket Engine. UARL Report E-910092-9, September 1966. Also issued as NASA CR-695.

4. Deissler, R. G.: Diffusion Approximation for Thermal Radiation in Gases with Jump Boundary Condition. Journal of Heat Transfer, Vol. 7, No. 4, 1967.

5. Krascella, N. L.: Theoretical Investigation of the Spectral Opacities of Hydrogen and Nuclear Fuel. Air Force Systems Command Report RTD-TDR-63-1101 prepared by UARL, November 1963.

6. Krascella, N. L.: Theoretical Investigation of the Opacity of Heavy-Atom Gases. UARL Report D-910092-4, September 1965.

7. Waber, J. T., D. Liberman and D. T. Cromer: Private communication, Los Alamos Scientific Laboratory, Los Alamos, New Mexico, June 1966.

8. Williamson, H. A., H. H. Michels and S. B. Schneiderman: Theoretical Investigation of the Lowest Five Ionization Potentials of Uranium, UARL Report D-910099-2, September 1965.

9. Krascella, N. L.: Theoretical Investigation of the Absorptive Properties of Small Particles and Heavy-Atom Gases. UARL Report E-910092-7, September 1966.

10. Corliss, C. H. and W. R. Bozman: Experimental Transition Probabilities for Spectral Lines of Seventy Elements. NBS Monograph 53, Washington 25, D. C., July 20, 1962.

11. Kies, C. C., C. J. Humphreys, and D. C. Laun: Preliminary Description and Analysis of the First Spectrum of Uranium. Journal of Research of the National Bureau of Standards, Research Paper RP 1729, Vol. 27, July 1946.

12. Bennett, H. E. et al: Infrared Reflectance of Aluminum Evaporated in Ultra-High Vacuum. Journal of the Optical Society of America, Vol. 53, No. 9, p. 1089, September 1968.

13. Cole, T. T. and F. Oppenheimer: Polarization by Reflection and Some Optical Constants in the Extreme Ultraviolet. Applied Optics, Vol. 1, p. 709, 1962.

14. Madden, R. P. et al: On the Vacuum Ultraviolet Reflectance of Evaporated Aluminum Before and During Oxidation. Journal of the Optical Society of America, Vol. 53, No. 5, p. 620, May 1963.

15. Hass, G. et al: Influence of Purity, Substrate Temperature and Aging Conditions on the Extreme Ultraviolet Reflectance of Evaporated Aluminum. Journal of the Optical Society of America, Vol. 47, No. 12, p. 1070, December 1957.

LIST OF SYMBOLS

a_R Rosseland Mean Opacity, cm^{-1}

a_ω Spectral absorption coefficient, cm^{-1}

P Pressure, atm

Q Total flux or integrated flux, Btu/ft^2-sec or erg/cm^2-sec

Q_ω Spectral flux, erg/cm-sec

Q* Black-body flux (for temperature T*) $= \sigma T^{*4}$, Btu/ft^2-sec

r_ω Spectral reflectivity, dimensionless

T Temperature, ^oR or ^oK

T* Effective black-body radiating temperature (taken as $15{,}000^oR$ for all cases considered).

T_E Edge-of-fuel temperature (see Eqs. (2) and (3)), ^oR

y Distance from edge of fuel (measured from edge of fuel toward the center line or away from end wall), cm

λ Wavelength, $\mathring{A}$ or microns (μ)

ω Wave number, cm^{-1}

ρ Mass density, lb/ft^3

τ Optical depth, dimensionless

Subscripts and Superscripts

bb Refers to a black-body property

F Fuel

T Total

ω Wave number or spectral quantity

TABLE I

SUMMARY OF CONDITIONS AND APPROXIMATIONS
USED IN VARIOUS CASES

Total Pressure, $P_T = P_{FUEL} + P_{NEON} + P_{SEED} = 500$ Atm

Case	Ionization Potentials *	Heavy-Atom Model **	Reflectivities	Seeding	Effective Radiating Temperature $T^* = {}^oR$	Edge-of-Fuel Temperature $T_E = {}^oR$
1	LOW	CONT	ZERO	NONE	15,000	10,650
2	HIGH	CONT	ZERO	NONE	15,000	10,650
3	LOW	BAND	ZERO	NONE	15,000	10,650
4	LOW	BAND	ZERO	10 atm hydrogen	15,000	10,650
5	LOW	CONT	Uniform see Fig. 4	NONE	15,000	14,650
6	LOW	CONT	Aluminum see Fig. 4	NONE	15,000	19,650

* HIGH - Refers to fuel ionization potentials of 6.1, 17.1, 38.8 and 65.6 ev - see Ref. 8
LOW - Refers to fuel ionization potentials of 6.1, 11.46, 17.94 and 31.14 ev - see Ref. 7

** CONT - Refers to heavy-atom model with continuum approximation for oscillator strengths in line region of the spectrum - see Refs. 5 and 6
BAND - Refers to heavy-atom model with band approximation for oscillator strengths in line region of the spectrum - see Ref. 9

FIG. 1

UNIT CAVITY OF A NUCLEAR LIGHT BULB ENGINE

OVERALL ENGINE EMPLOYS SEVEN UNIT CAVITIES SIMILAR TO CAVITY SHOWN

y MEASURED RADIALLY INWARD FROM EDGE OF FUEL FOR CASES 1 THROUGH 4; AXIALLY FROM EDGE OF FUEL FOR CASES 5 AND 6

ALL DIMENSIONS IN FEET

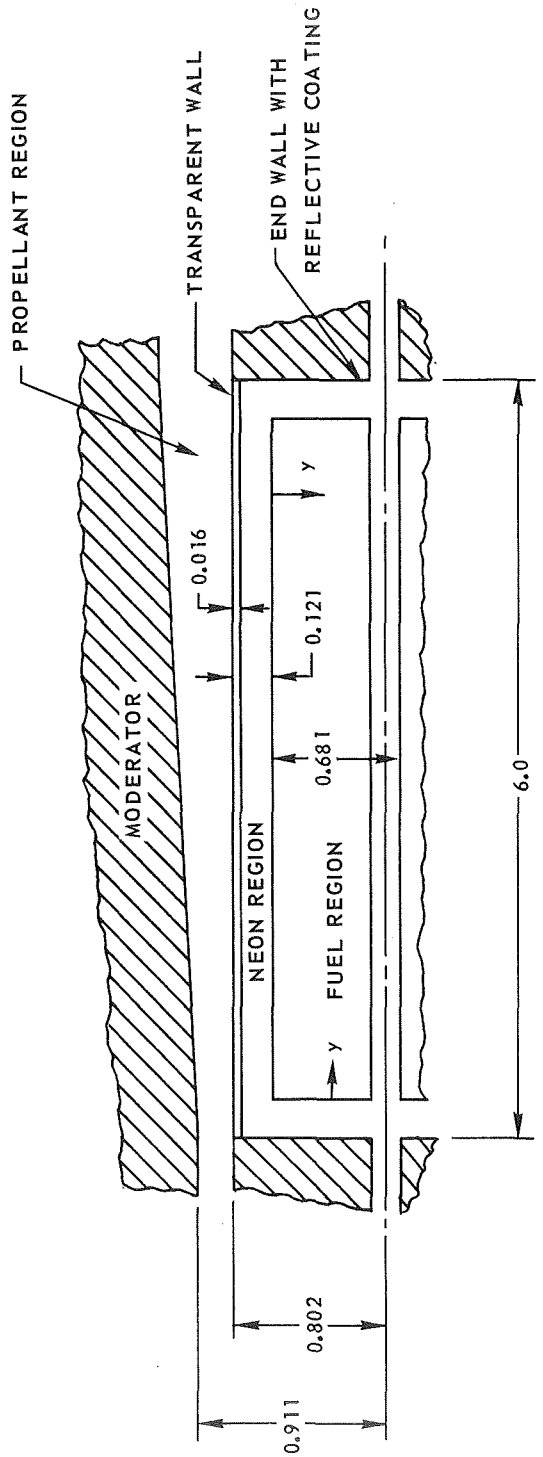

FIG. 2

ASSUMED NUCLEAR FUEL PARTIAL PRESSURE DISTRIBUTION

$$P_F = \begin{cases} 19.271\,y + 0.01 & y \leq 10.378 \\ 2.0 \times 10^2 & y > 10.378 \end{cases} \text{ ATM}$$

NOTE: $\begin{cases} P_{NEON} = 500 - P_{SEED}\,\beta\,P_{FUEL} \\ \text{TOTAL PRESSURE} = 500 \text{ ATM} \end{cases}$

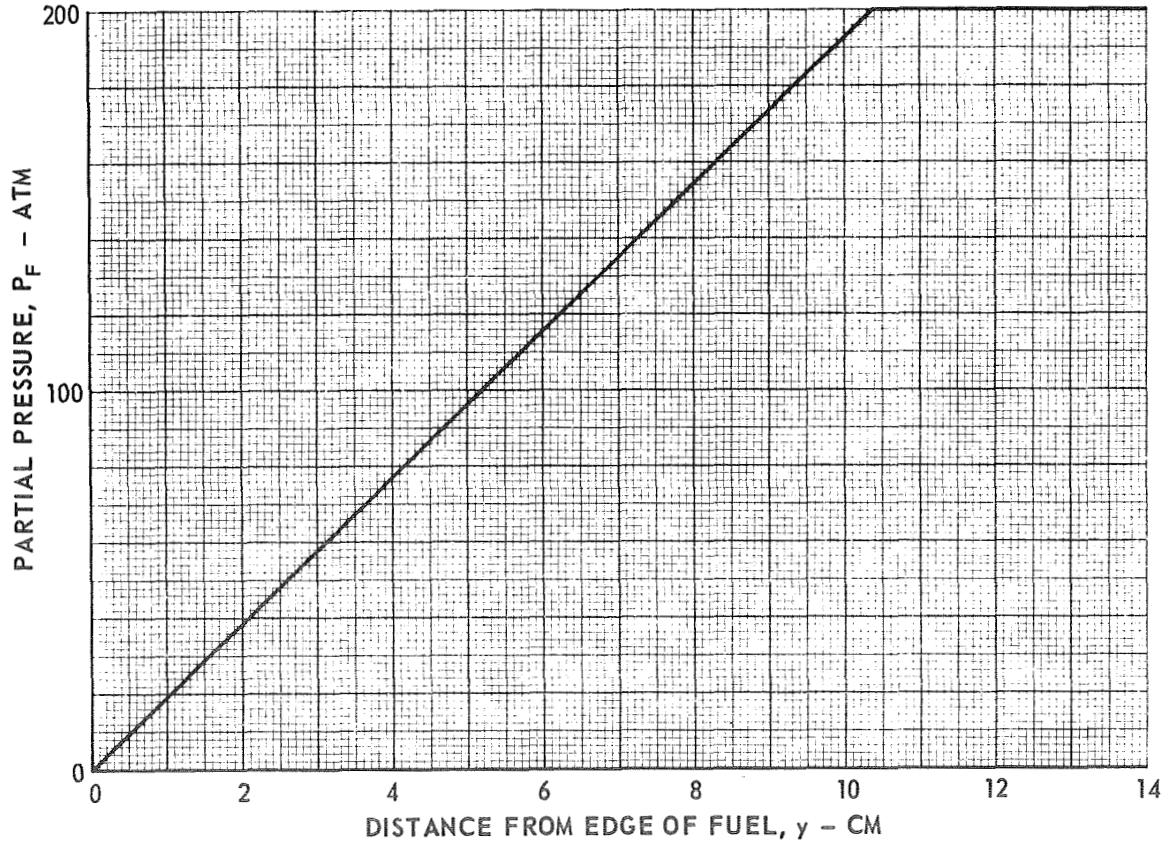

FIG. 3

OSCILLATOR STRENGTH DISTRIBUTION FOR THE BOUND–BOUND REGION OF HEAVY–ATOM MODEL USED FOR CASES 3 AND 4

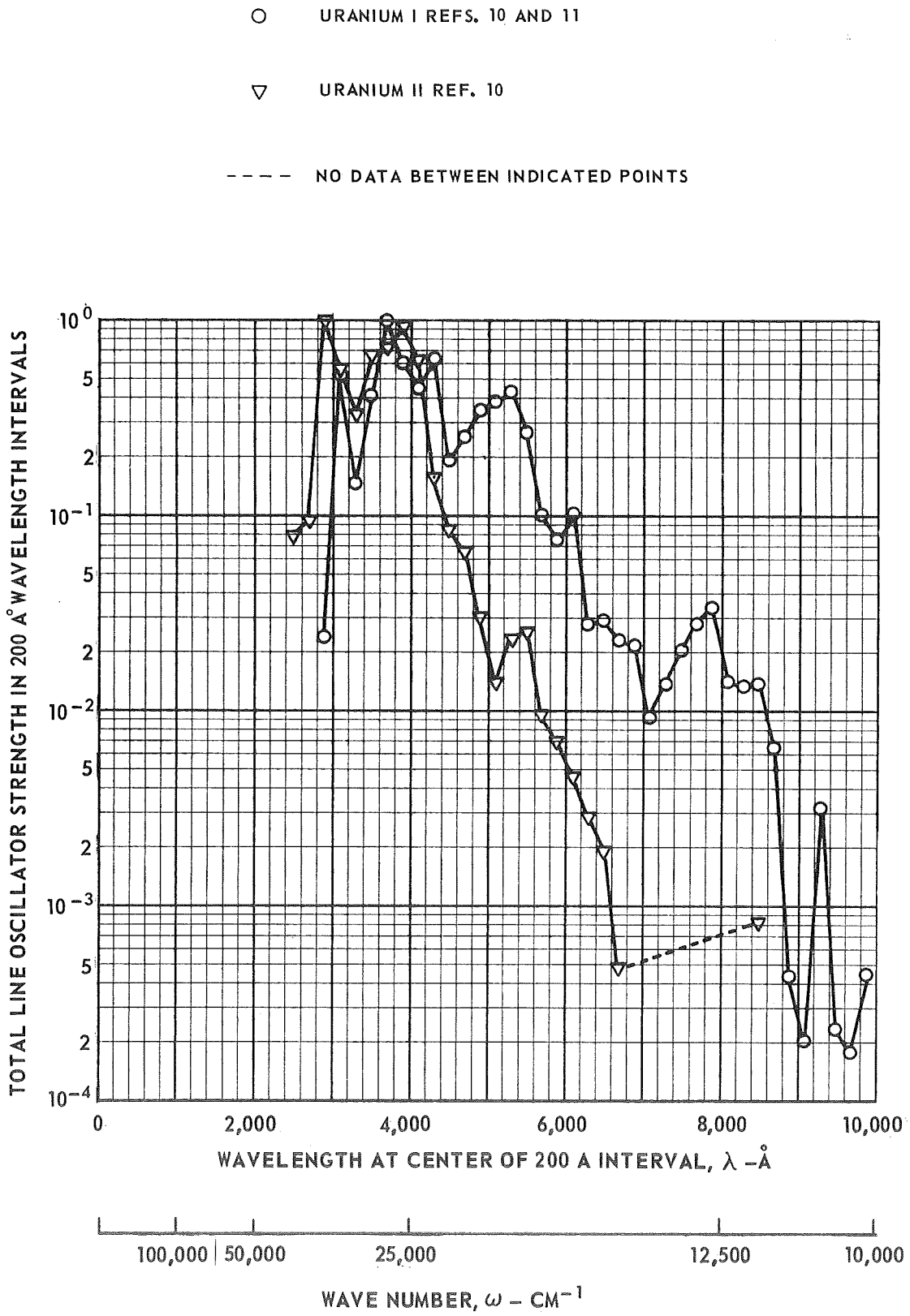

FIG. 4

SPECTRAL REFLECTIVITY OF ALUMINUM AND UNIFORM REFLECTIVITY USED IN CASES 5 AND 6

CASE	SYMBOL	REFERENCES
5	- - - - - - -	—
6 (ALUMINUM)	□	12
	△	13
	▽	14
	○	15

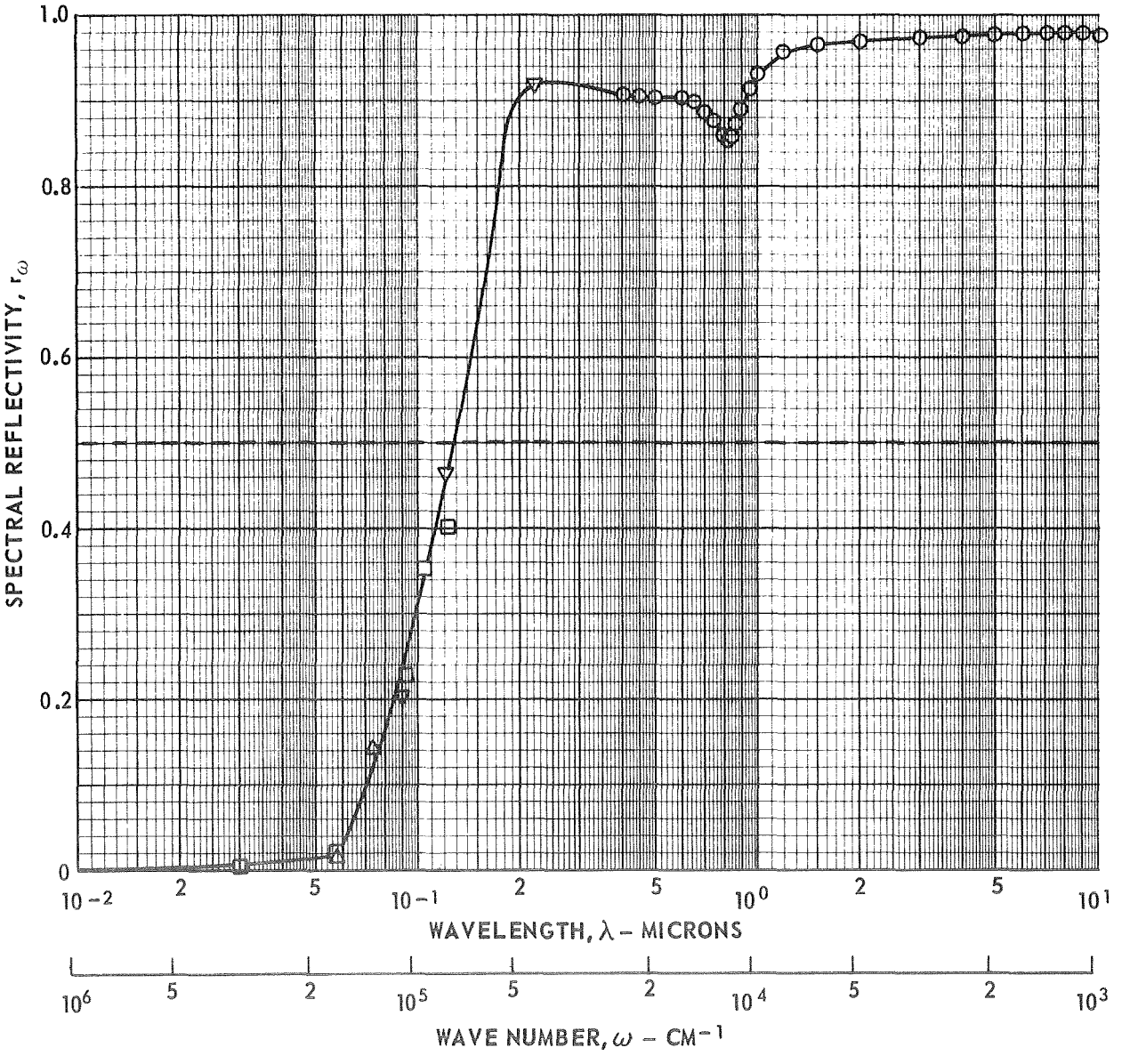

FIG. 5

TOTAL FLUX DISTRIBUTIONS IN OUTER LAYER OF FUEL REGION

CASE	IP	MODEL	T_E – °R	SEED	r_ω
1	LOW	CONT	10,650	NONE	0
2	HIGH	CONT	10,650	NONE	0
3	LOW	BAND	10,650	NONE	0
4	LOW	BAND	10,650	10 ATM HYDROGEN	0
5	LOW	CONT	14,650	NONE	UNIFORM
6	LOW	CONT	19,650	NONE	ALUMINUM

$T^* = 15{,}000\,°R$

$Q^* = 24{,}300\ BTU/FT^2\text{-}SEC$

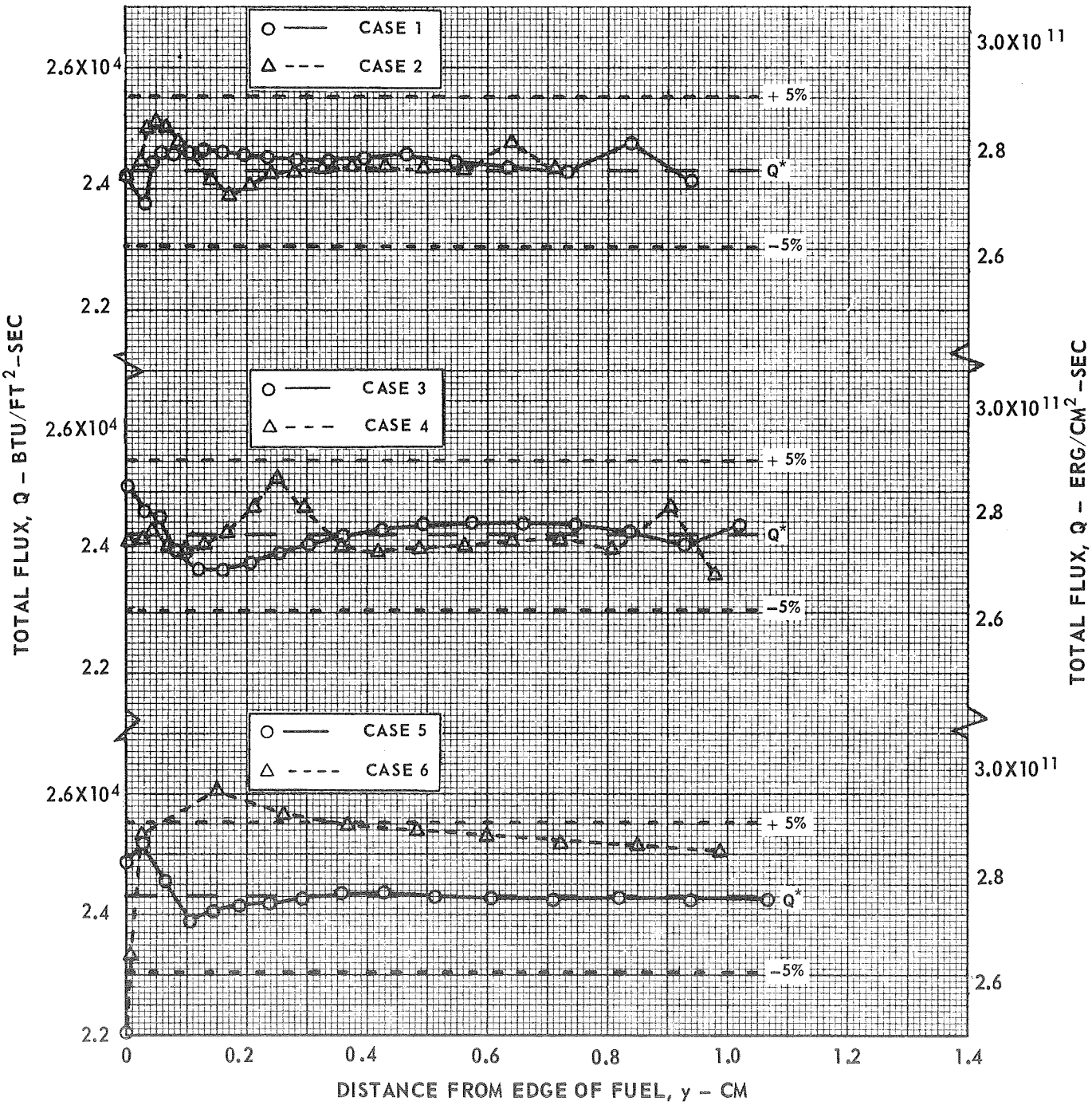

FIG. 6

TEMPERATURE DISTRIBUTION IN OUTER LAYER OF FUEL REGION FOR VARIOUS CASES

CASE	SYMBOL	I P	MODEL	SEED	r_ω
1	———	LOW	CONT	NONE	0
2	- - - - -	HIGH	CONT	NONE	0
3	— · —	LOW	BAND	NONE	0
4	— ··· —	LOW	BAND	10 ATM–H_2	0
5	———	LOW	CONT	NONE	UNIFORM
6	———	LOW	CONT	NONE	ALUMINUM

$T^* = 15{,}000°\ R$

$Q^* = 24{,}300\ BTU/FT^2\text{–}SEC$

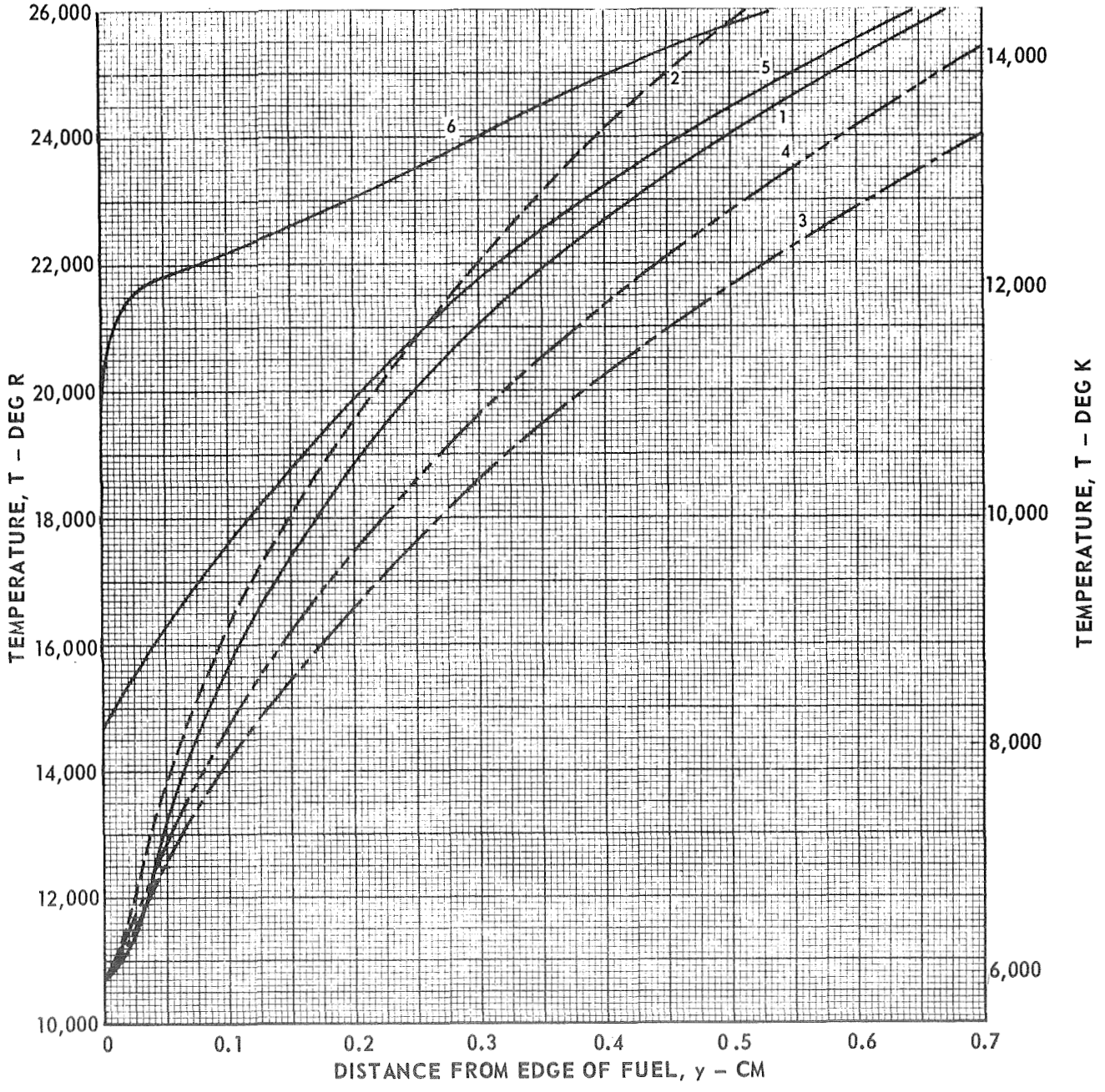

FIG. 7

COMPARISON OF SPECTRAL ABSORPTION COEFFICIENT OF NUCLEAR FUEL AT EDGE-OF-FUEL CONDITIONS USED IN CASES 1, 2 AND 3

CASE	SYMBOL	IP	MODEL
1	- - - - - -	LOW	CONT
2	— - —	HIGH	CONT
3	———	LOW	BAND

$T^* = 15{,}000\,^\circ R$

$Q^* = 24{,}300$ BTU/FT^2 – SEC

$T_E = 10{,}650\,^\circ R$

$r_\omega = 0$

$P_F = 0.01$ atm

SEEDS – NONE

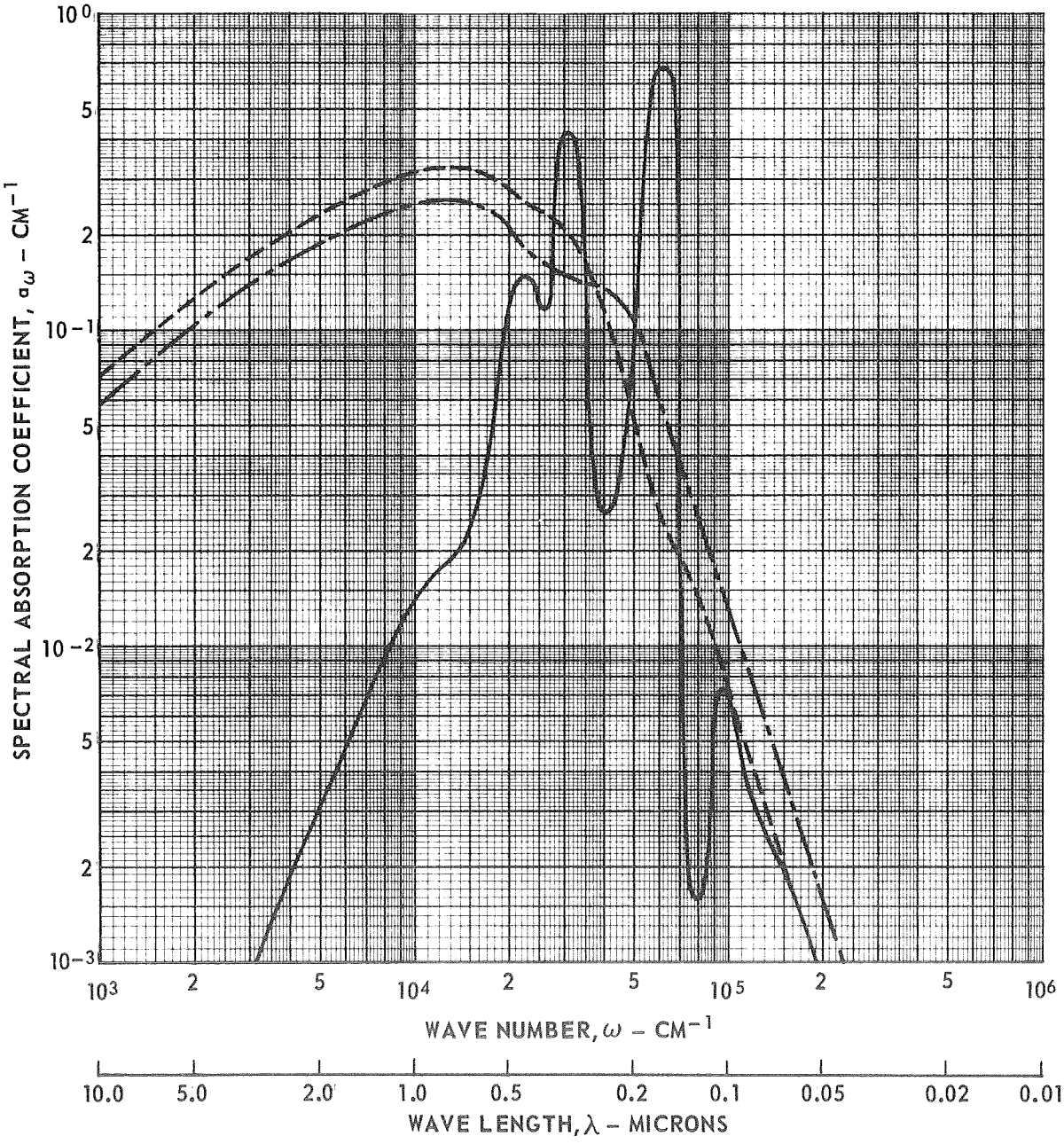

FIG. 8

COMPARISON OF SPECTRAL ABSORPTION COEFFICIENTS OF NUCLEAR FUEL AND HYDROGEN SEED AT EDGE-OF-FUEL CONDITIONS USED IN CASES 3 AND 4

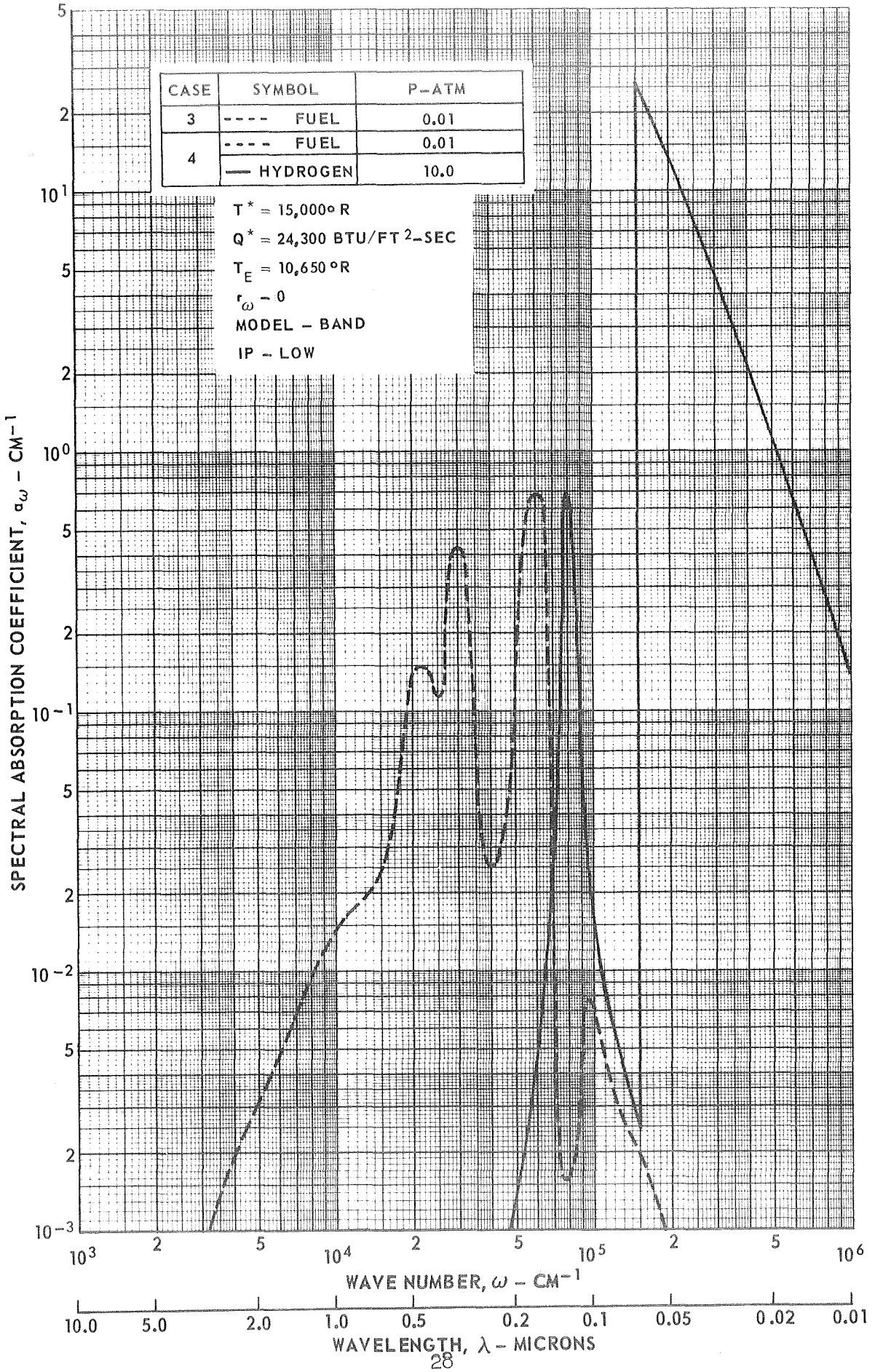

FIG. 9

COMPARISON OF SPECTRAL ABSORPTION COEFFICIENTS OF NUCLEAR FUEL AT EDGE-OF-FUEL CONDITIONS USED IN CASE 1, 5 AND 6

CASE	SYMBOL	T_E - °R	r_ω
1	- - - - -	10,650	0
5	———	14,650	UNIFORM
6	—·—	19,650	ALUMINUM

T^* = 15,000 °R
Q^* = 24,300 BTU/FT^2-SEC
P_F = 0.01 ATM
MODEL - CONT
IP - LOW
SEEDS - NONE

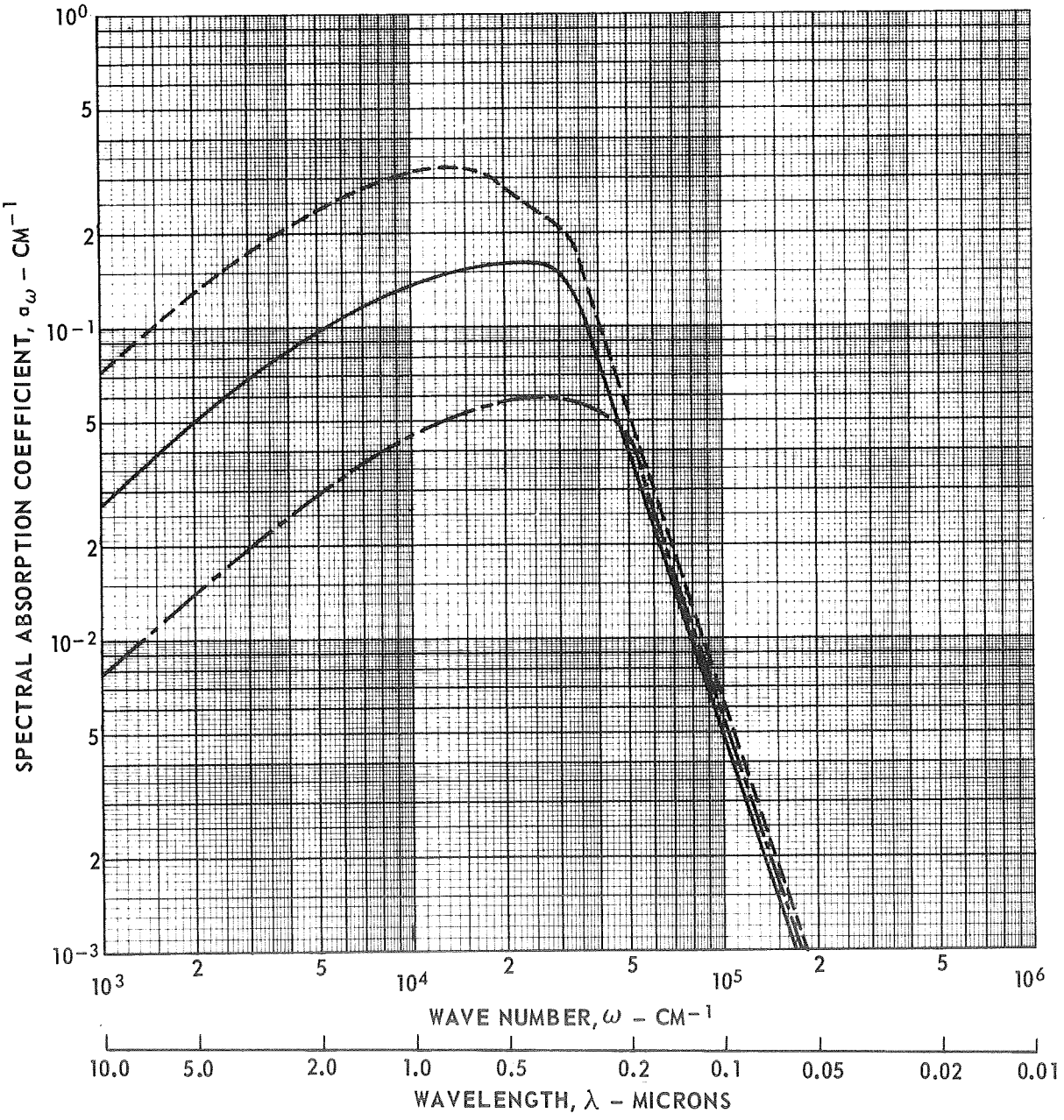

FIG. 10

COMPARISON OF NUCLEAR FUEL MASS DENSITY DISTRIBUTIONS FOR CASES 1, 2 AND 3

CASE	SYMBOL	IP	MODEL
1	———	LOW	CONT
2	- - - - - - -	HIGH	CONT
3	— - - —	LOW	BAND

$T^* = 15{,}000^\circ R$

$Q^* = 24{,}300$ BTU/FT^2-SEC

$T_E = 10{,}650^\circ R$

$r_\omega = 0$

SEEDS – NONE

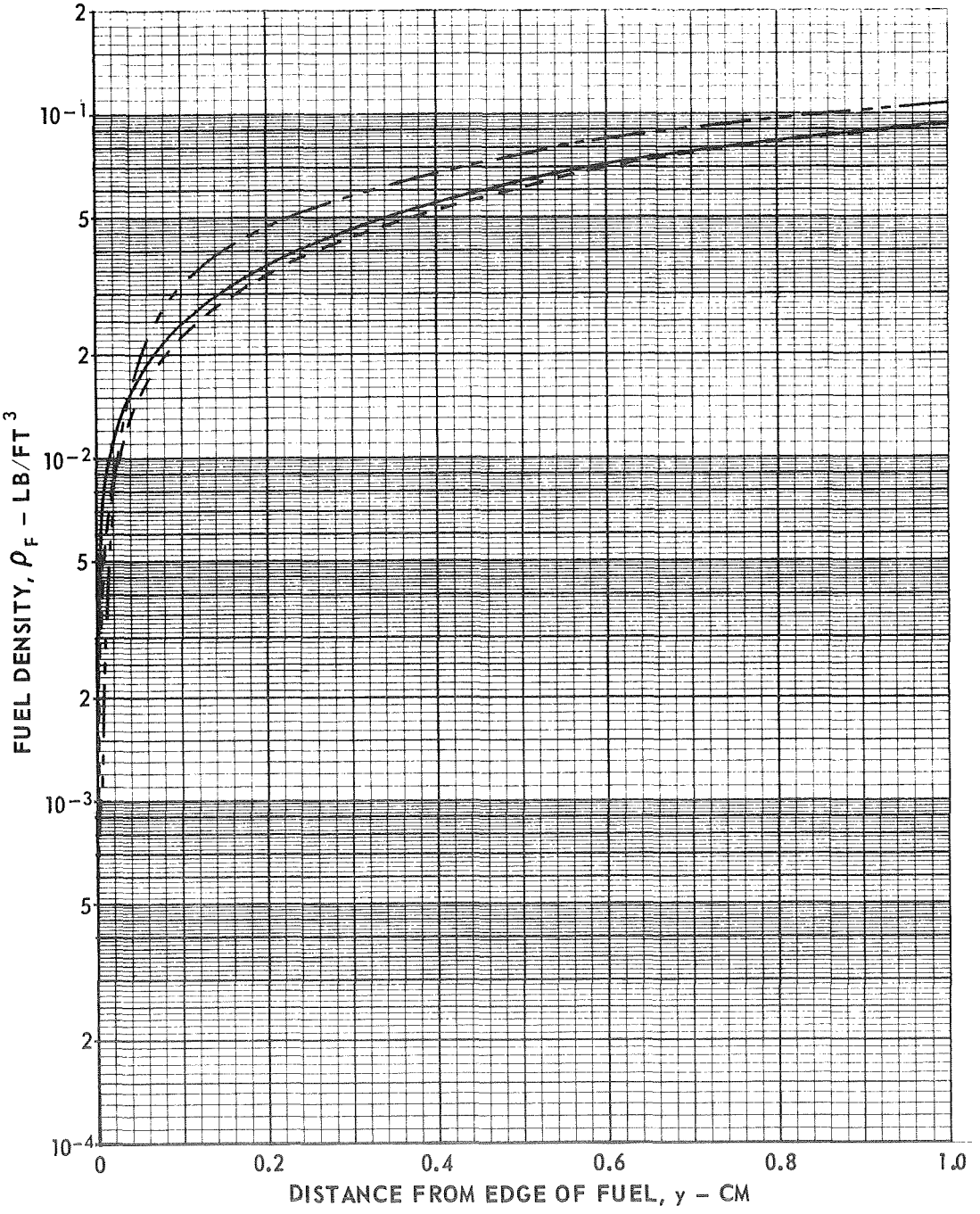

FIG. 11

COMPARISON OF NUCLEAR MASS DENSITY DISTRIBUTIONS FOR CASES 3 AND 4

CASE	SYMBOL	SEED
3	— -- —	NONE
4	———	10.0 ATM HYDROGEN

$T^* = 15{,}000^\circ R$

$Q^* = 24{,}300$ BTU/FT^2-SEC

$T_E = 10{,}650^\circ R$

$\zeta_\omega - 0$

MODEL-BAND

IP - LOW

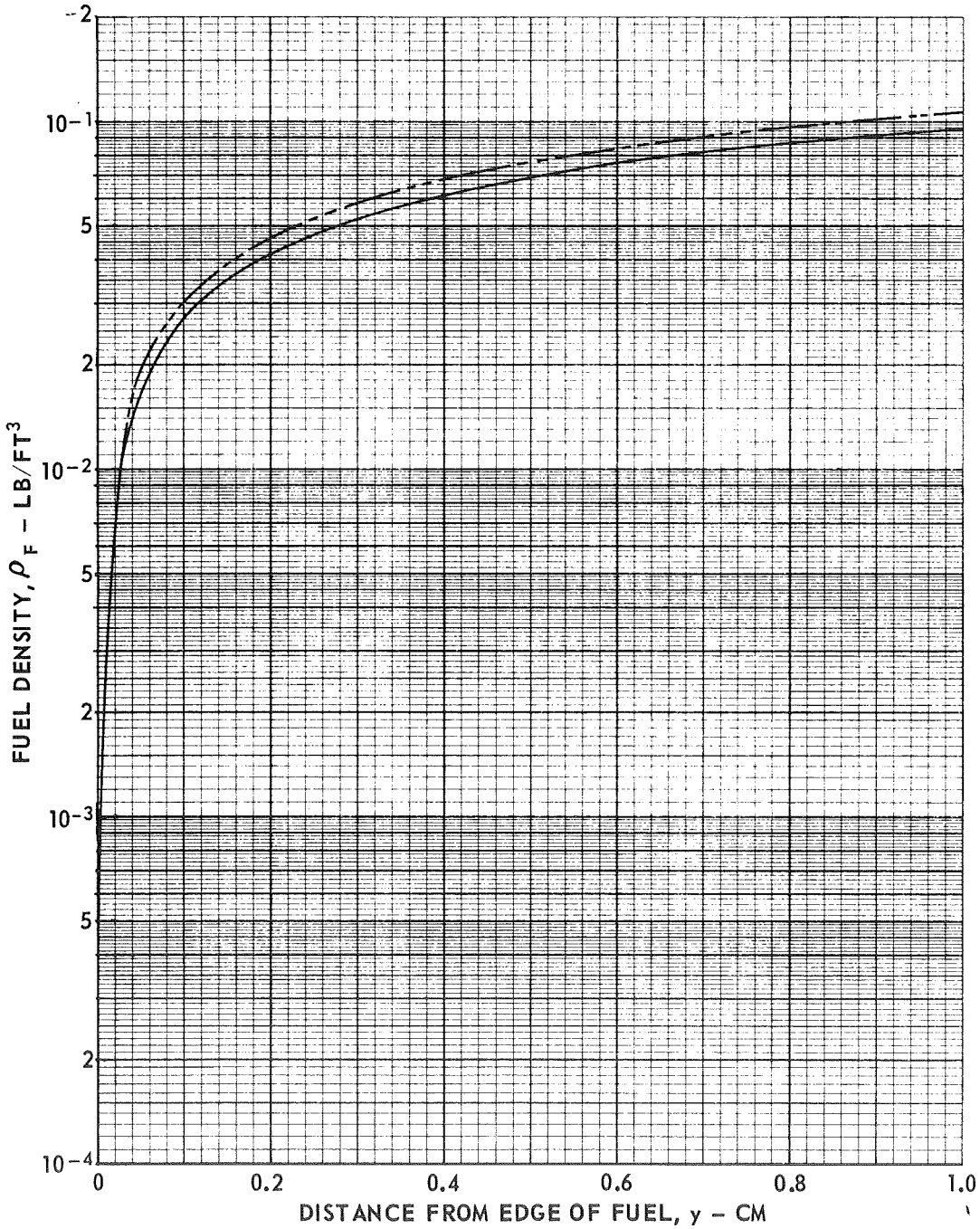

FIG. 12

COMPARISON OF NUCLEAR FUEL MASS DENSITY DISTRIBUTIONS FOR CASES 1, 5 AND 6

CASE	SYMBOL	T_E – °R	r_ω
1	———	10,650	0
5	- - - - - -	14,650	UNIFORM
6	— · · —	19,650	ALUMINUM

T^* = 15,000° R
Q^* = 24,300 BTU/FT^2-SEC
MODEL – CONT
IP – LOW
SEEDS – NONE

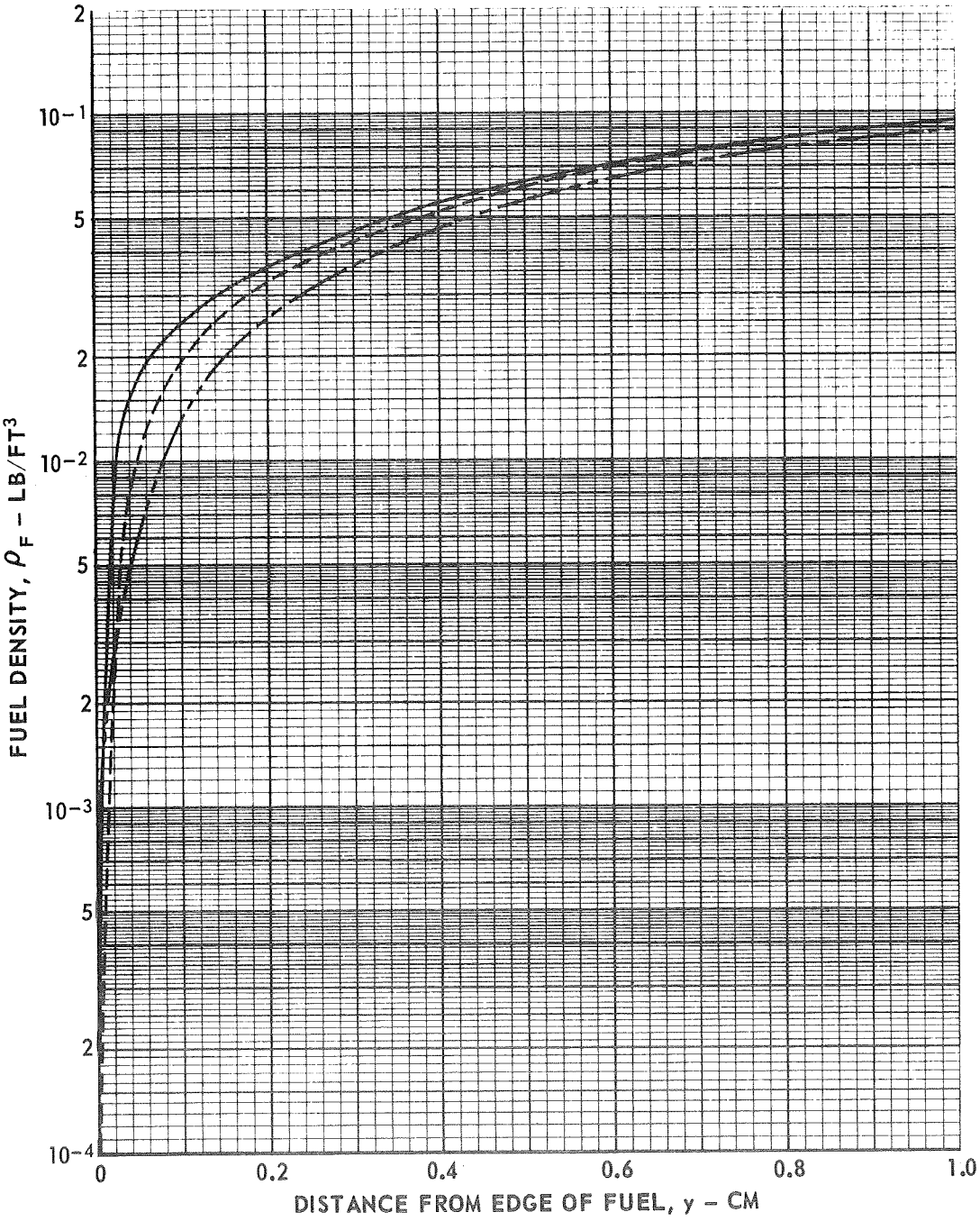

FIG. 13

COMPARISON OF TOTAL MASS DENSITY DISTRIBUTIONS FOR CASES 1, 2 AND 3

CASE	SYMBOL	IP	MODEL
1	———	LOW	CONT
2	- - - - - - -	HIGH	CONT
3	— - - —	LOW	BAND

$T^* = 15{,}000^\circ R$

$Q^* = 24{,}300$ BTU/FT^2-SEC

$T_E = 10{,}650^\circ R$

$r_\omega - 0$

SEEDS - NONE

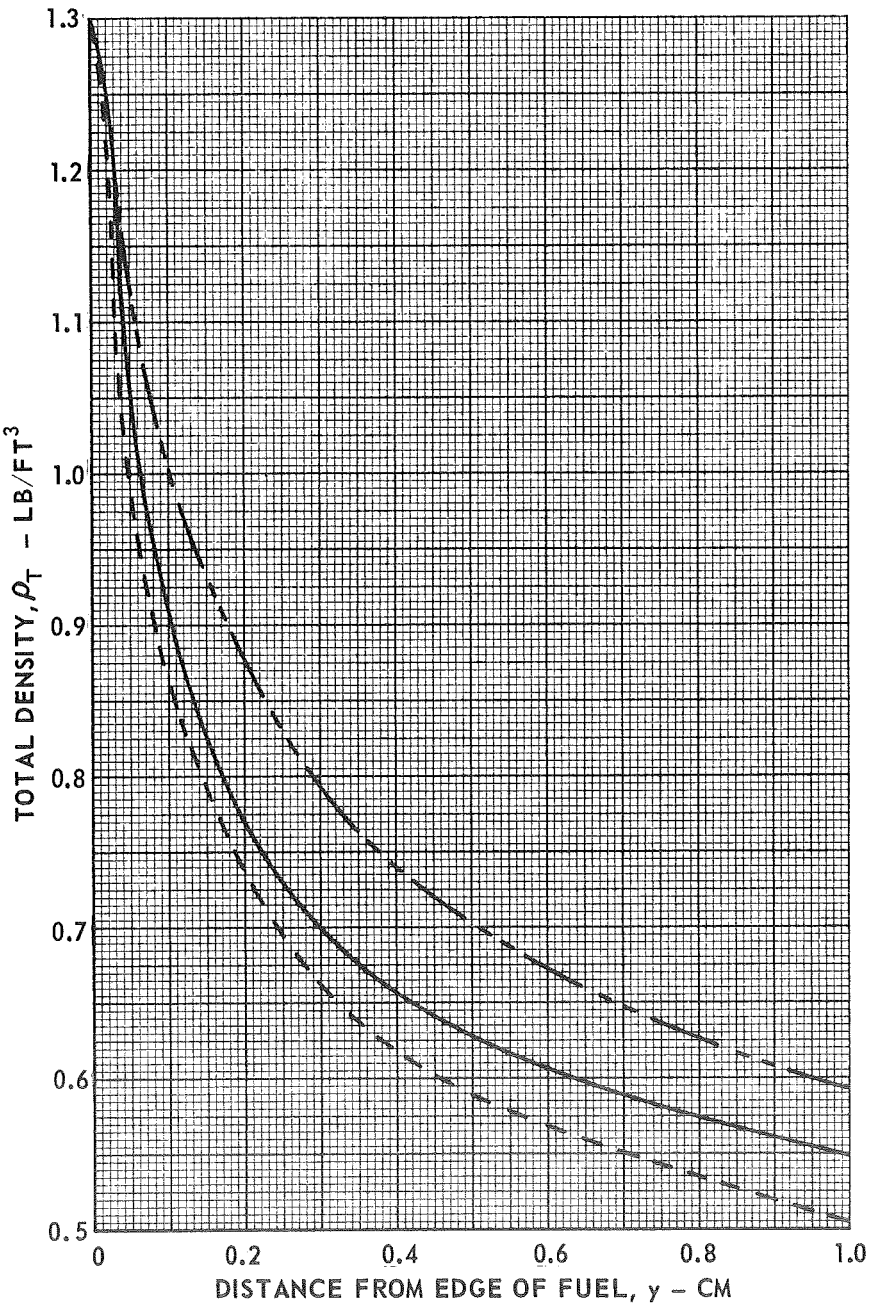

FIG. 14

COMPARISON OF TOTAL MASS DENSITY DISTRIBUTIONS FOR CASES 3 AND 4

CASE	SYMBOL	SEED
3	— — —	NONE
4	———	10.0 ATM HYDROGEN

$T^* = 15{,}000\,^\circ R$
$Q^* = 24{,}300$ BTU/FT^3-SEC
$T_E = 10{,}650\,^\circ R$
$r_\omega = 0$
MODEL-BAND
IP-LOW

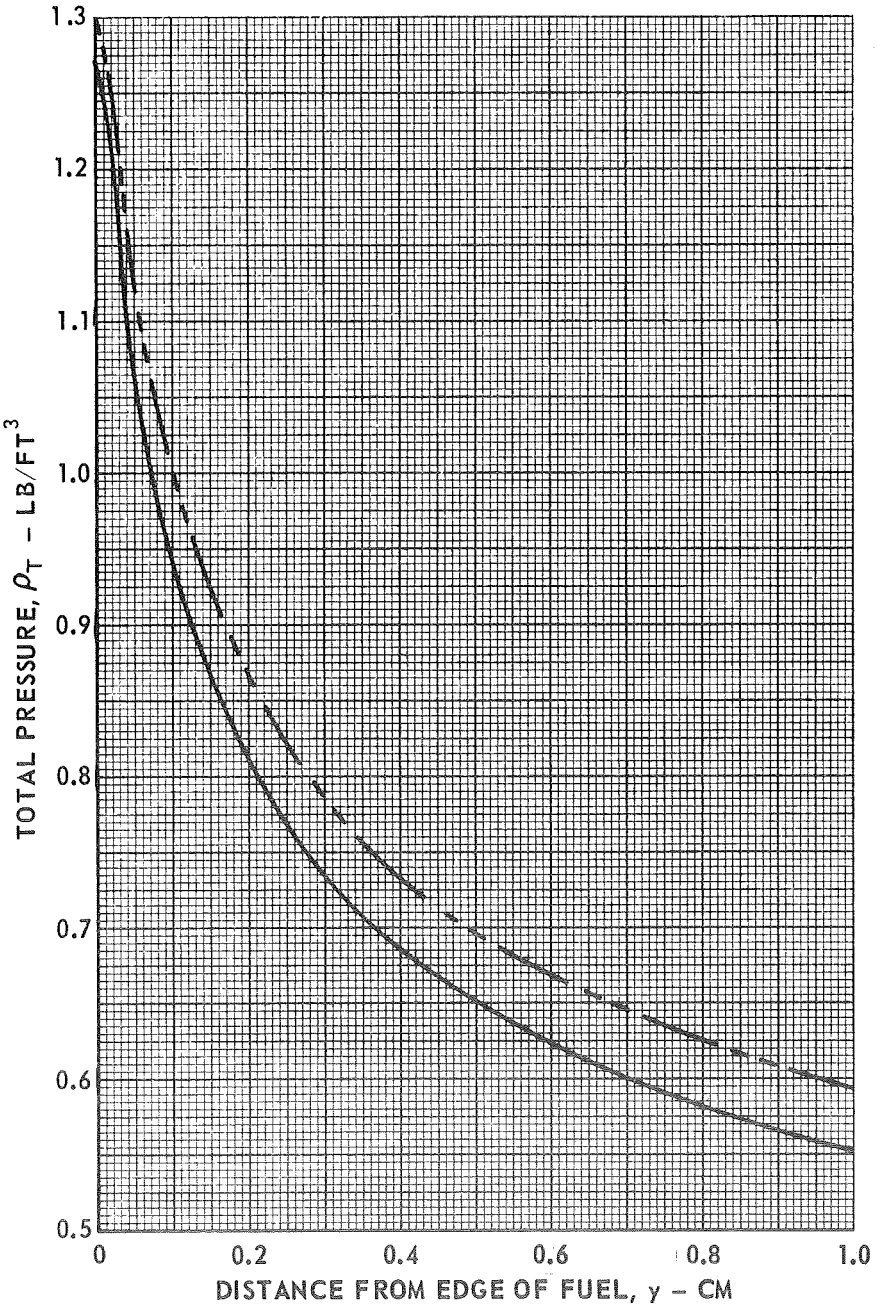

FIG. 15

COMPARISON OF TOTAL MASS DENSITY DISTRIBUTIONS FOR CASES 1, 5 AND 6

CASE	SYMBOL	T_E – °R	r_ω
1	———	10,650	0
5	- - - - - -	14,650	UNIFORM
6	—·—·—	19,600	ALUMINUM

$T^* = 15{,}000\ ^\circ R$
$Q^* = 24{,}300\ BTU/FT^2\text{-}SEC$
MODEL – CONT
IP – LOW
SEEDS – NONE

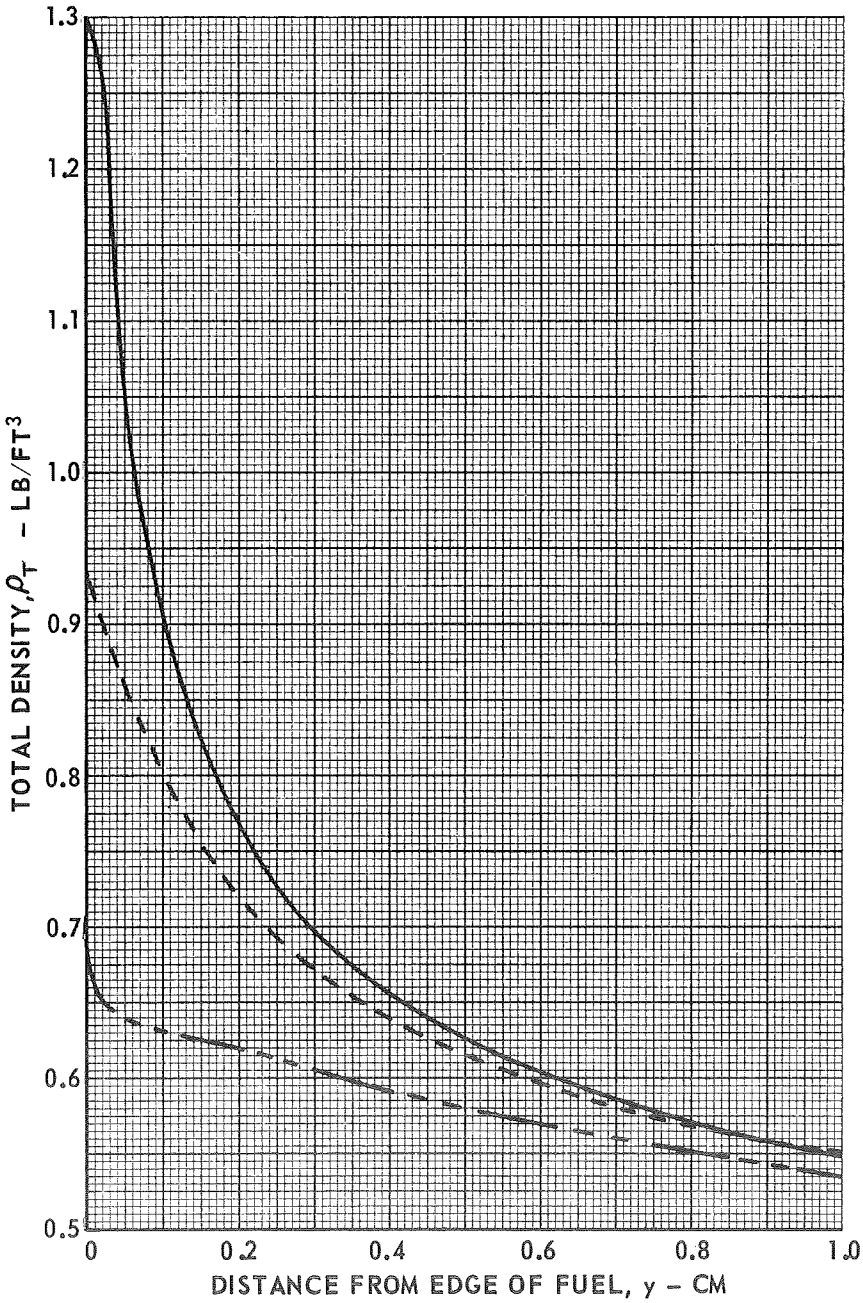

FIG. 16

COMPARISON OF SPECTRAL FLUX FOR BLACK BODY AT TEMPERATURES OF 10,000, 15,000 AND 20,000 DEG R AND SPECTRAL FLUX EMITTED FROM NUCLEAR FUEL FOR CASES 1, 2 AND 3

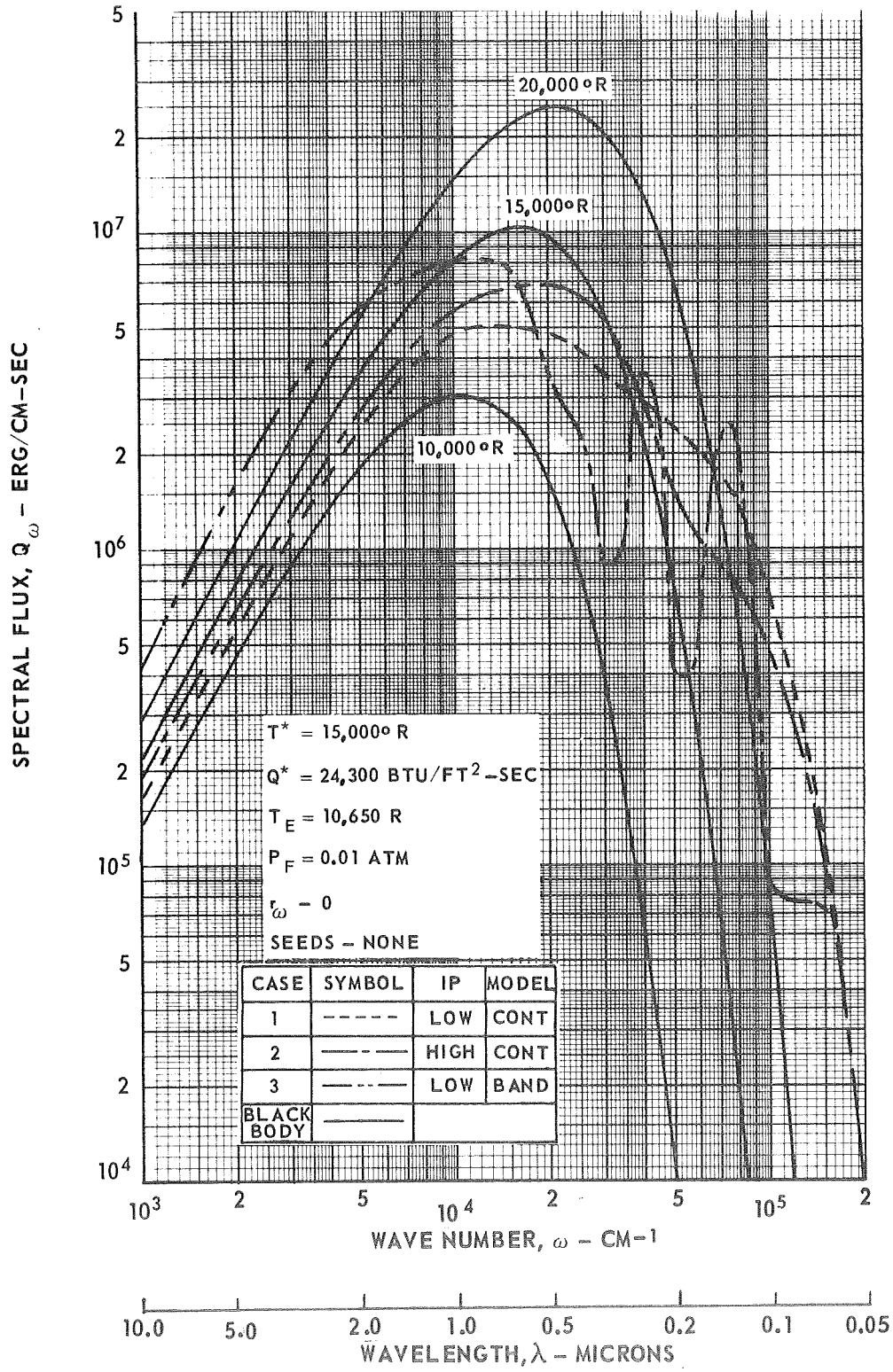

FIG. 17

COMPARISON OF RELATIVE FRACTIONAL FLUX DISTRIBUTION OF BLACK BODY AT TEMPERATURES OF 10,000 15,000 AND 20,000 DEG R AND RELATIVE FRACTIONAL FLUX DISTRIBUTION EMITTED FROM THE NUCLEAR FUEL FOR CASES 1, 2 AND 3

CASE	SYMBOL	I P	MODEL
1	- - - - -	LOW	CONT
2	— - - —	HIGH	CONT
3	— - —	LOW	BAND
BLACK BODY	———		

$T^* = 15{,}000°\ R$

$Q^* = 24{,}300\ BTU/FT^2\text{-}SEC$

$T_E = 10{,}650°\ R$

$P_F = 0.01\ ATM$

$r_\omega - 0$

SEEDS - NONE

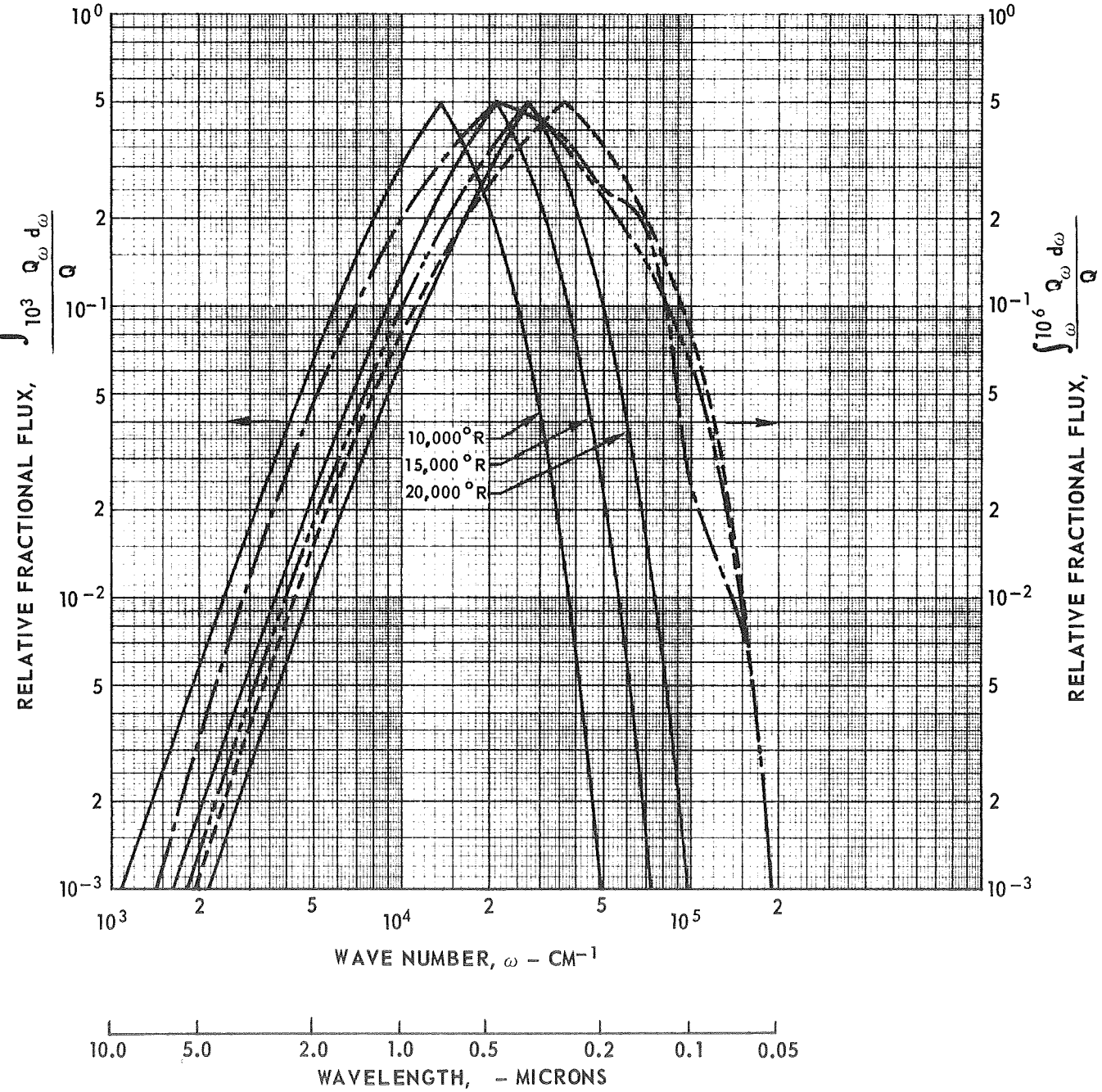

FIG. 18

COMPARISON OF SPECTRAL FLUX FOR BLACK BODY AT TEMPERATURES OF 10,000 15,000 AND 20,000 DEG R AND SPECTRAL FLUX EMITTED FROM NUCLEAR FUEL FOR CASES 3 AND 4

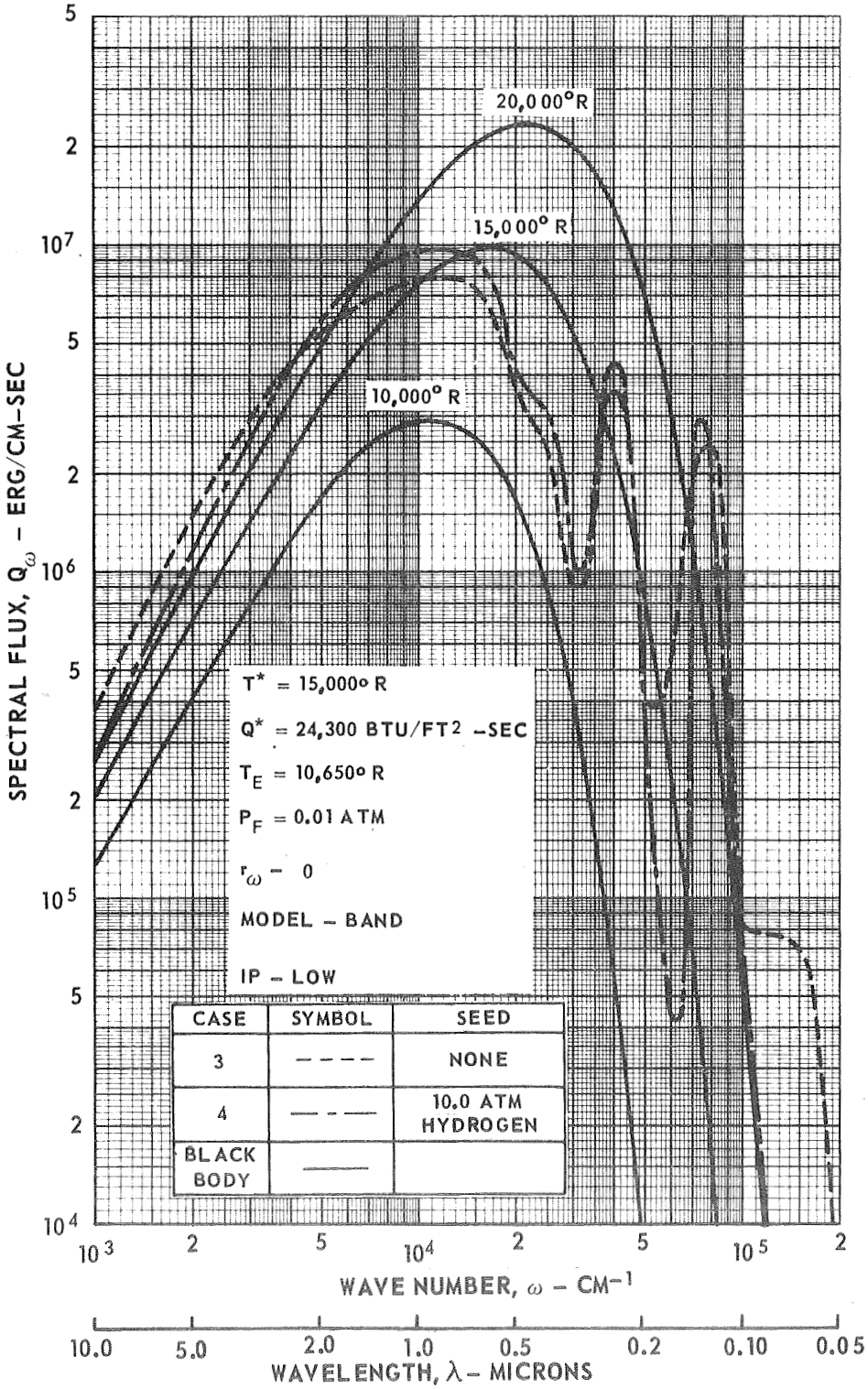

COMPARISON OF RELATIVE FRACTIONAL FLUX DISTRIBUTION OF BLACK BODY AT TEMPERATURES OF 10,000, 15,000 AND 20,000 DEG R AND RELATIVE FRACTIONAL FLUX DISTRIBUTION EMITTED FROM THE NUCLEAR FUEL FOR CASES 3 AND 4

CASE	SYMBOL	SEED
3	- - - - - -	NONE
4	— - —	10.0 ATM HYDROGEN
BLACK BODY	———	

$T^* = 15{,}000\,^\circ R$

$Q^* = 24{,}300$ BTU/FT^2-SEC

$T_E = 10{,}650\,^\circ R$

$P_F = 0.01$ ATM

$r_\omega - 0$

MODEL – BAND

IP – LOW

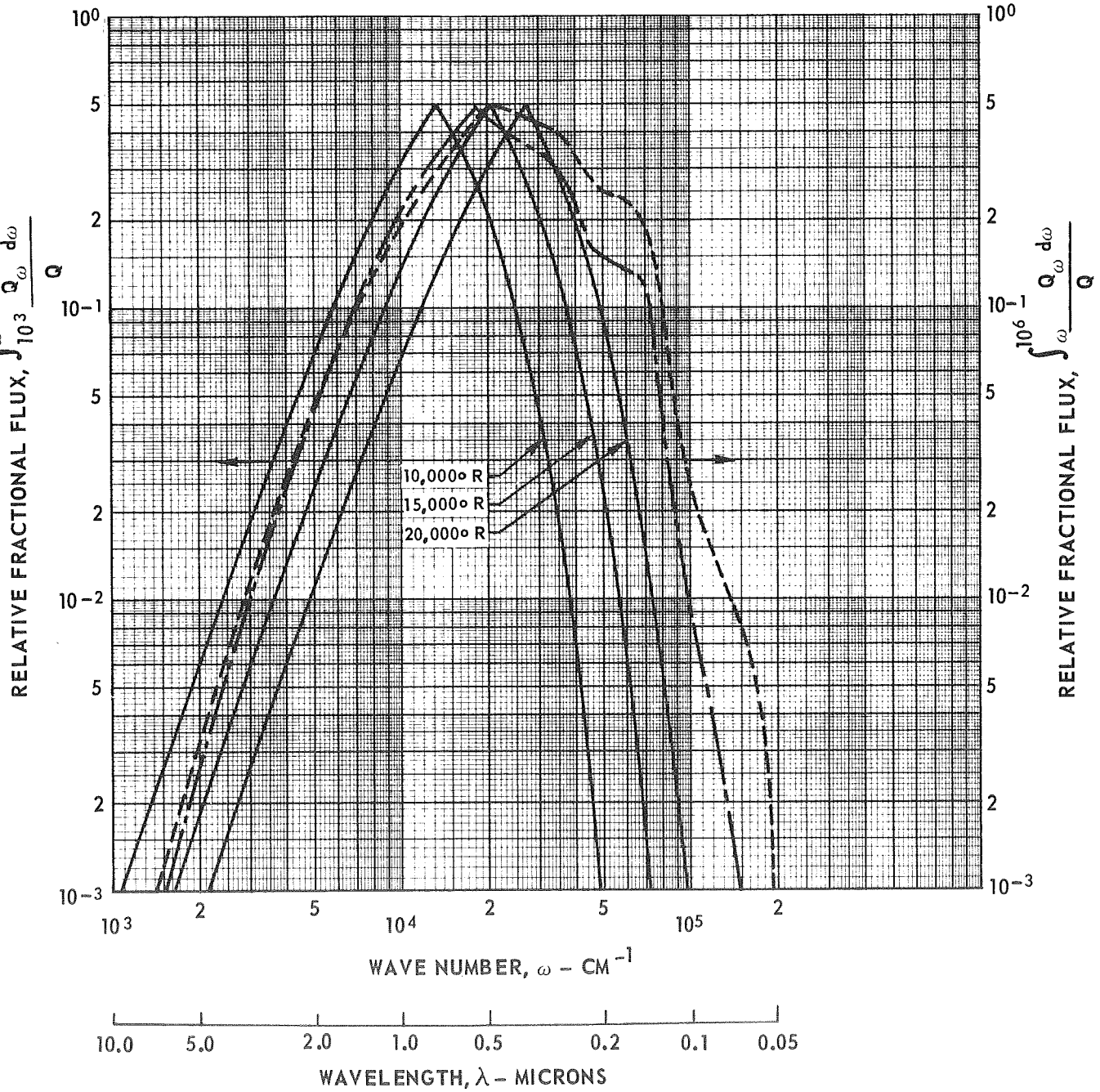

FIG. 20

COMPARISON OF SPECTRAL FLUX FOR BLACK BODY AT TEMPERATURES OF 10,000, 15,000 AND 20,000 DEG R AND SPECTRAL FLUX EMITTED FROM NUCLEAR FUEL FOR CASES 1, 5 AND 6

CASE	SYMBOL	T_E – °R	r_ω
1	—·—	10,650	0
5	- - - - - - -	14,650	UNIFORM
6	—·—·—	19,650	ALUMINUM
BLACK BODY	———		

$T^* = 15{,}000\ °R$

$Q^* = 24{,}300\ BTU/FT^2\text{-SEC}$

$P_F = 0.01\ ATM$

MODEL CONT

IP – LOW

SEEDS – NONE

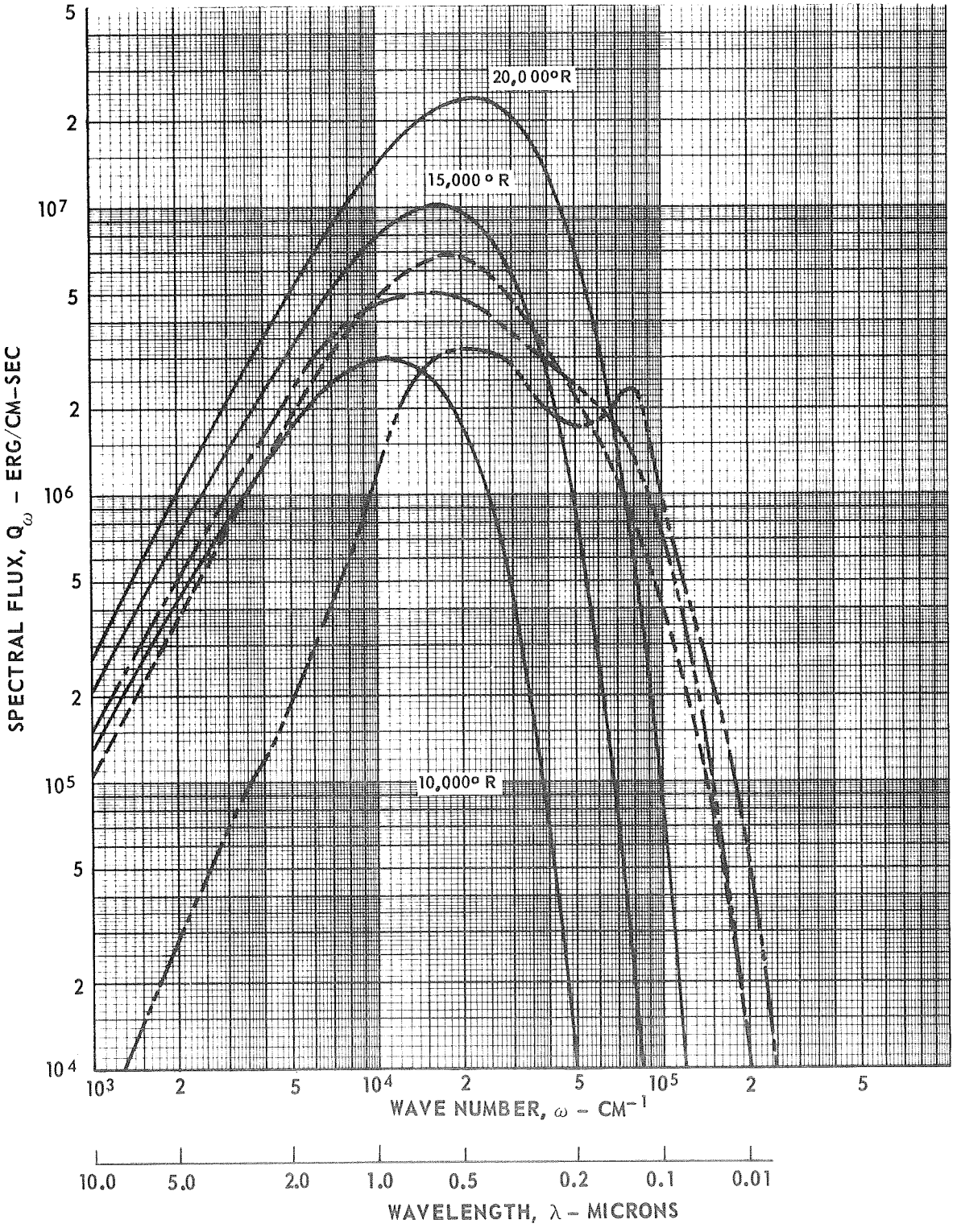

FIG. 21

COMPARISON OF RELATIVE FRACTIONAL FLUX DISTRIBUTION OF BLACK BODY AT TEMPERATURES OF 10,000, 15,000 AND 20,000 DEG R AND RELATIVE FRACTIONAL FLUX DISTRIBUTION EMITTED FROM THE NUCLEAR FUEL FOR CASES 1, 5 AND 6

CASE	SYMBOL	T_E – °R	r_ω
1	– – – – –	10,650	0
5	— – —	14,650	UNIFORM
6	— – · –	19,650	ALUMINUM
BLACK BODY	———		

$T^* = 15{,}000\ °R$

$Q^* = 24{,}300\ BTU/FT^2\text{-}SEC$

$P_F = 0.01\ ATM$

MODEL – CONT

SEEDS – NONE

IP – LOW

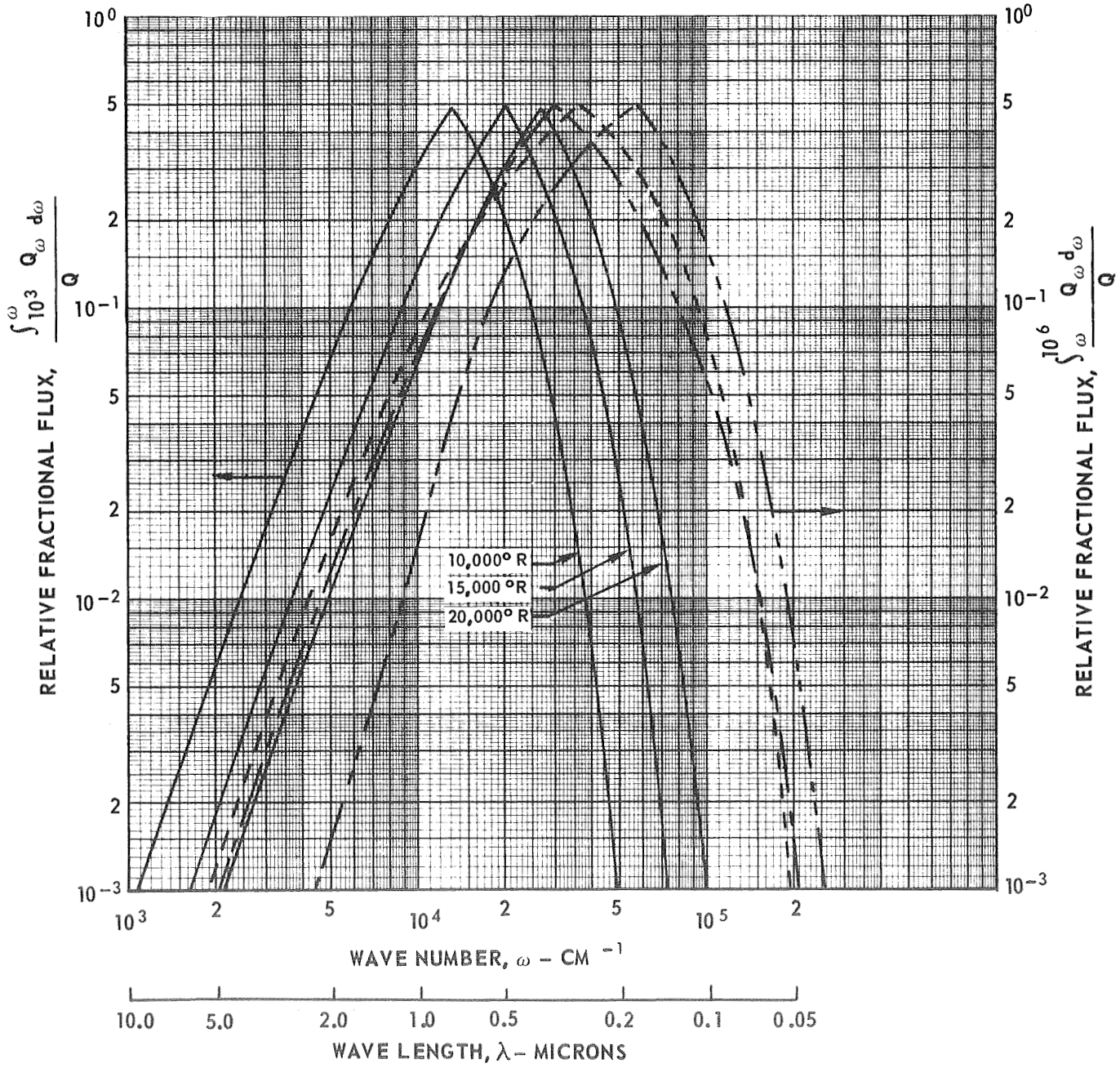

OPTICAL DEPTH DISTRIBUTION AT REPRESENTATIVE WAVE NUMBERS FOR CASE 1

$T^* = 15{,}000^\circ$ R

$Q^* = 24{,}300$ BTU/FT ^{2}-SEC

$$\tau_\omega = \int_0^y a_\omega \, dy$$

IP - LOW
MODEL - CONT
SEED - NONE
$r_\omega = 0$

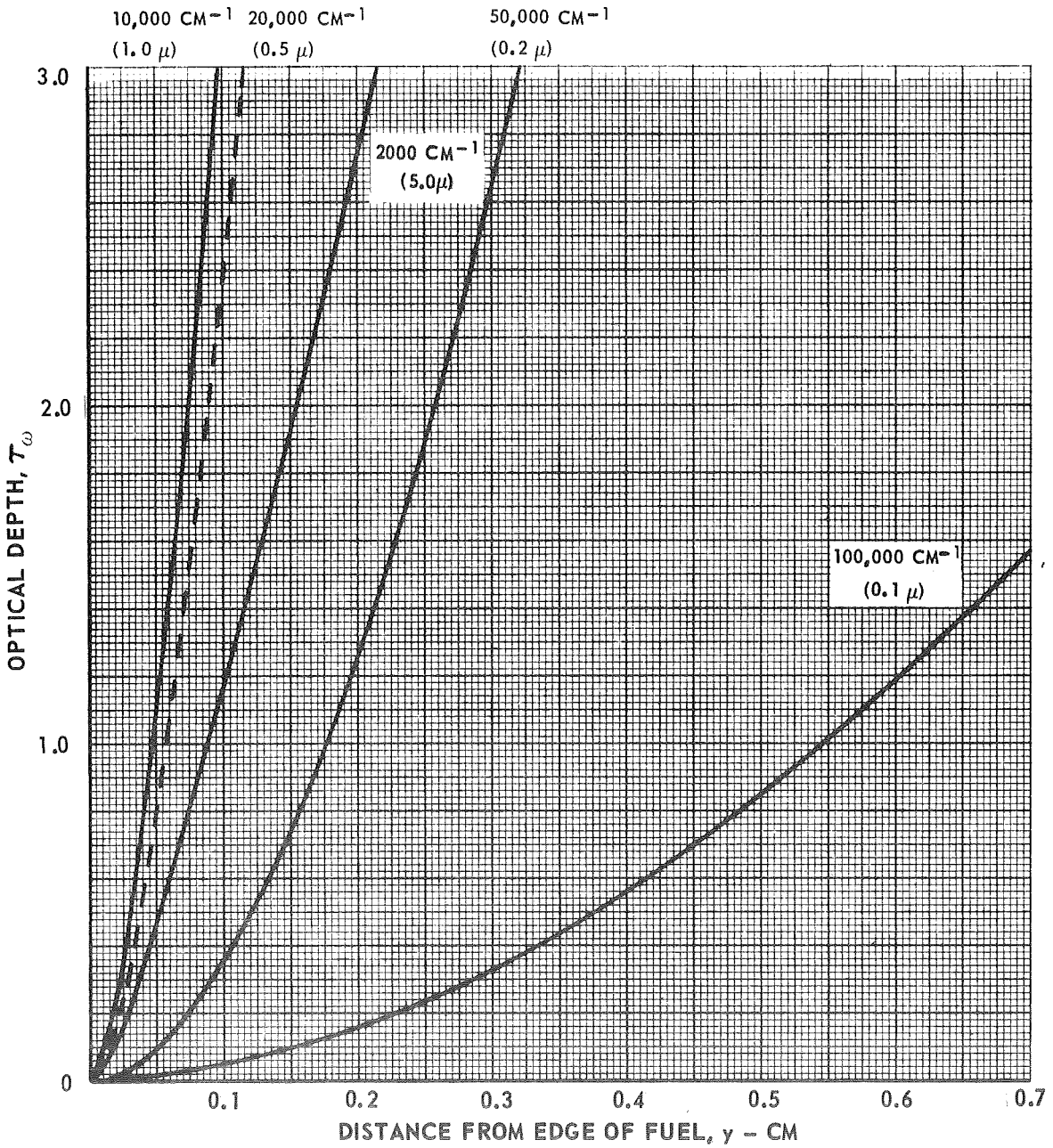

FIG. 23

OPTICAL DEPTH DISTRIBUTION AT REPRESENTATIVE WAVE NUMBERS FOR CASE 2

$T^* = 15{,}000\,^\circ R$
$Q^* = 24{,}300$ BTU/FT^2 SEC

$$\tau_\omega = \int_0^y a_\omega \, dy$$

IP – HIGH
MODEL – CONT
SEED – NONE
$r_\omega = 0$

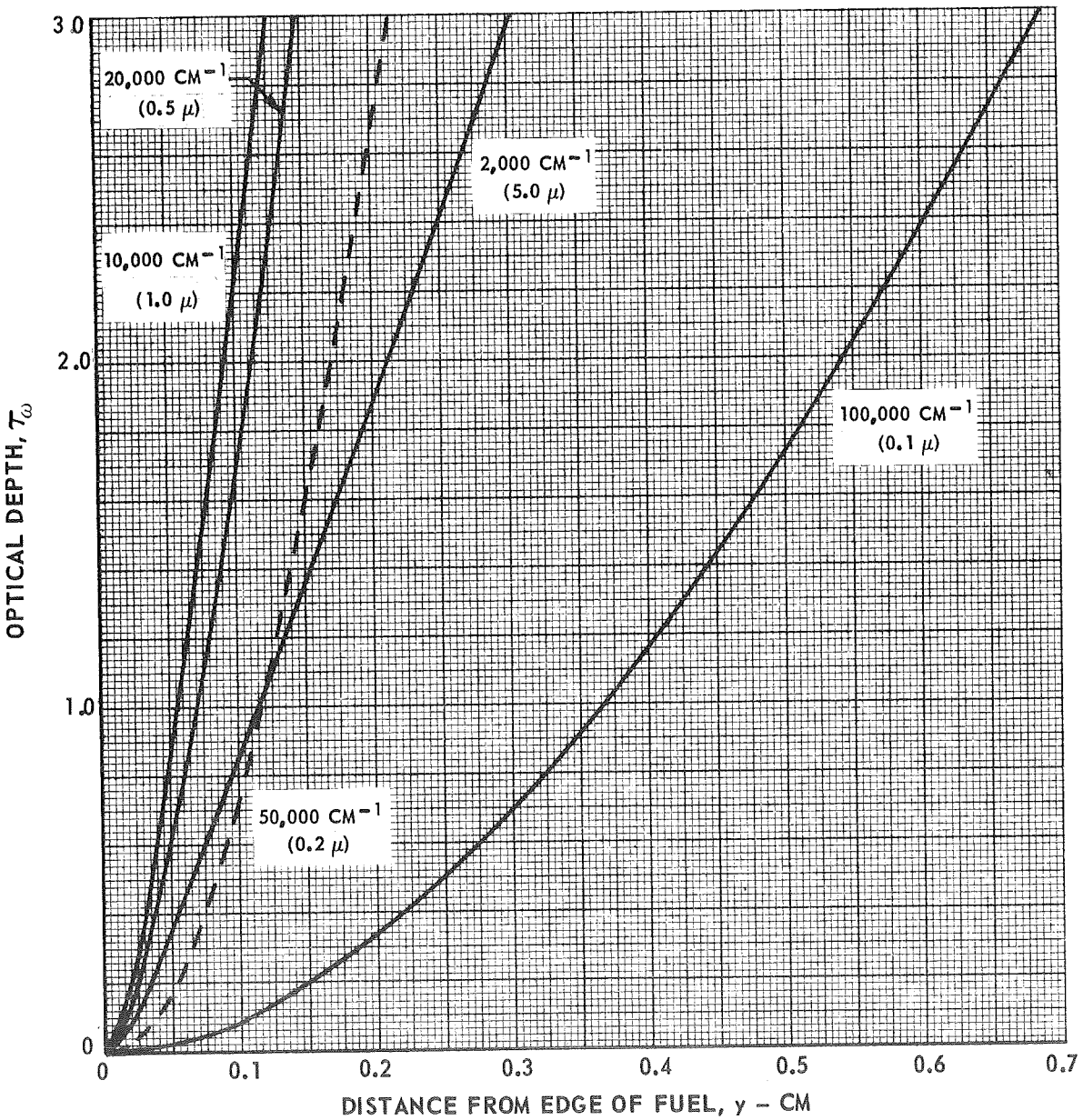

OPTICAL DEPTH DISTRIBUTION AT REPRESENTATIVE WAVE NUMBERS FOR CASE 3

$T^* = 15{,}000\,^\circ R$

$Q^* = 24{,}300\ BTU/FT^2\text{-}SEC$

$$\tau_\omega = \int_0^y a_\omega\, dy$$

IP - LOW
MODEL - BAND
SEED - NONE
$r_\omega = 0$

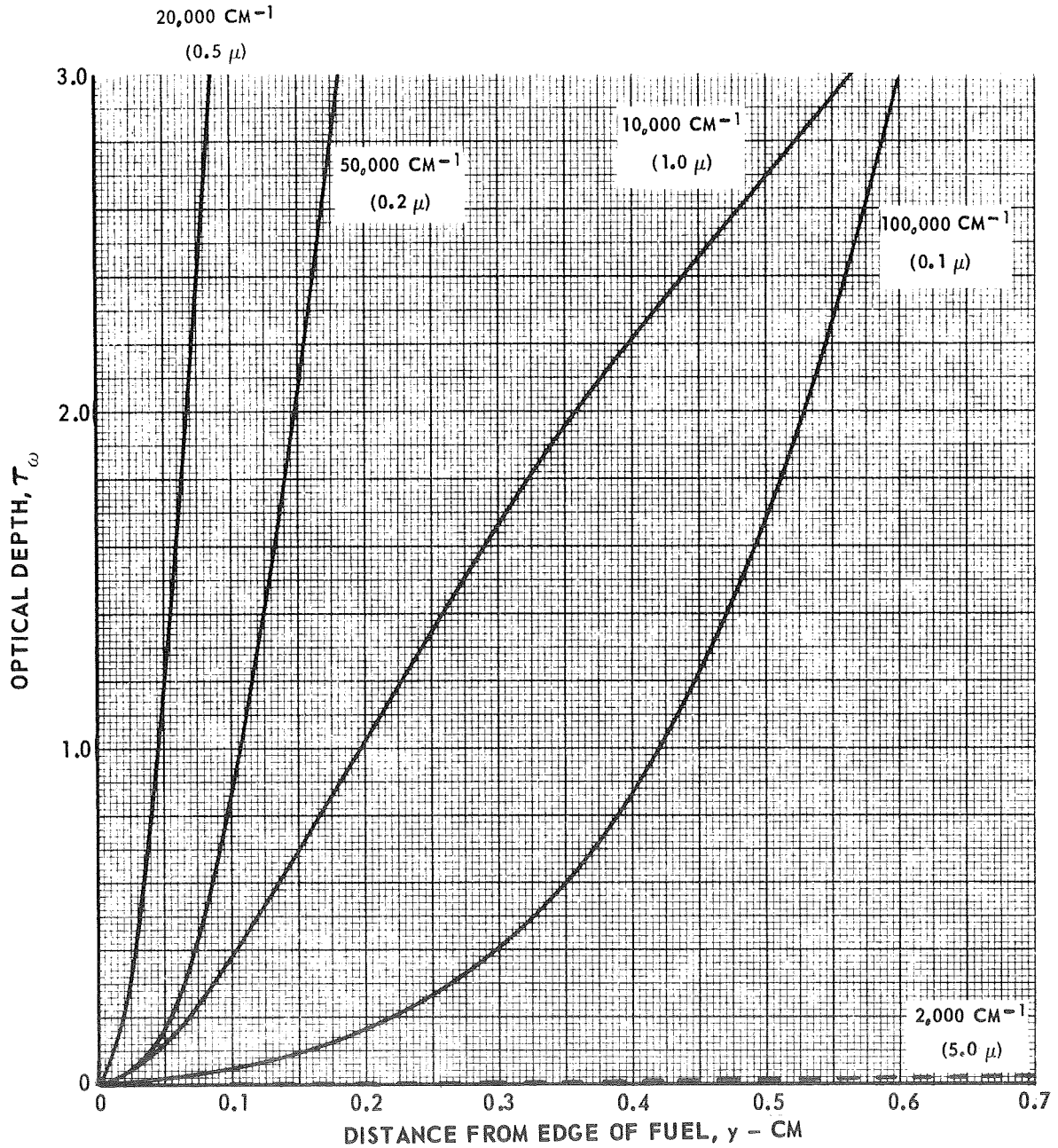

OPTICAL DEPTH DISTRIBUTION AT REPRESENTATIVE WAVE NUMBERS FOR CASE 4

$T^* = 15{,}000\,^\circ R$

$Q^* = 24{,}300$ BTU/FT^2-SEC

$$\tau_\omega = \int_0^y a_\omega \, dy$$

IP - LOW

MODEL - BAND

SEED - 10.0 ATM HYDROGEN

$r_\omega = 0$

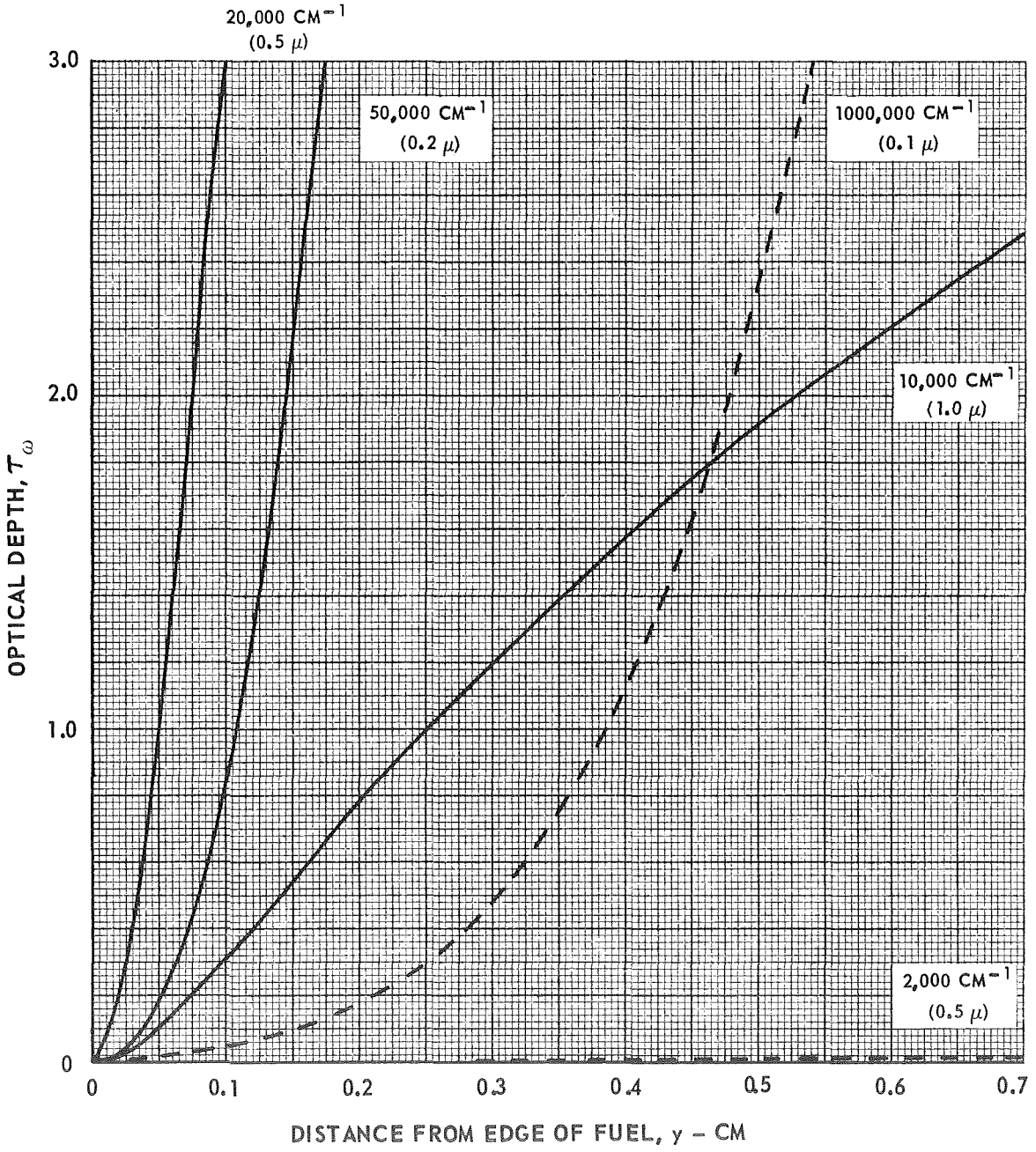

OPTICAL DEPTH DISTRIBUTION AT REPRESENTATIVE WAVE NUMBERS FOR CASE 5

$T^* = 15{,}000^\circ R$
$Q^* = 24{,}300\ BTU/FT^2\text{-}SEC$

$$\tau_\omega = \int_0^y a_\omega\, dy$$

IP – LOW
MODEL – CONT
SEED – NONE
r_ω – UNIFORM

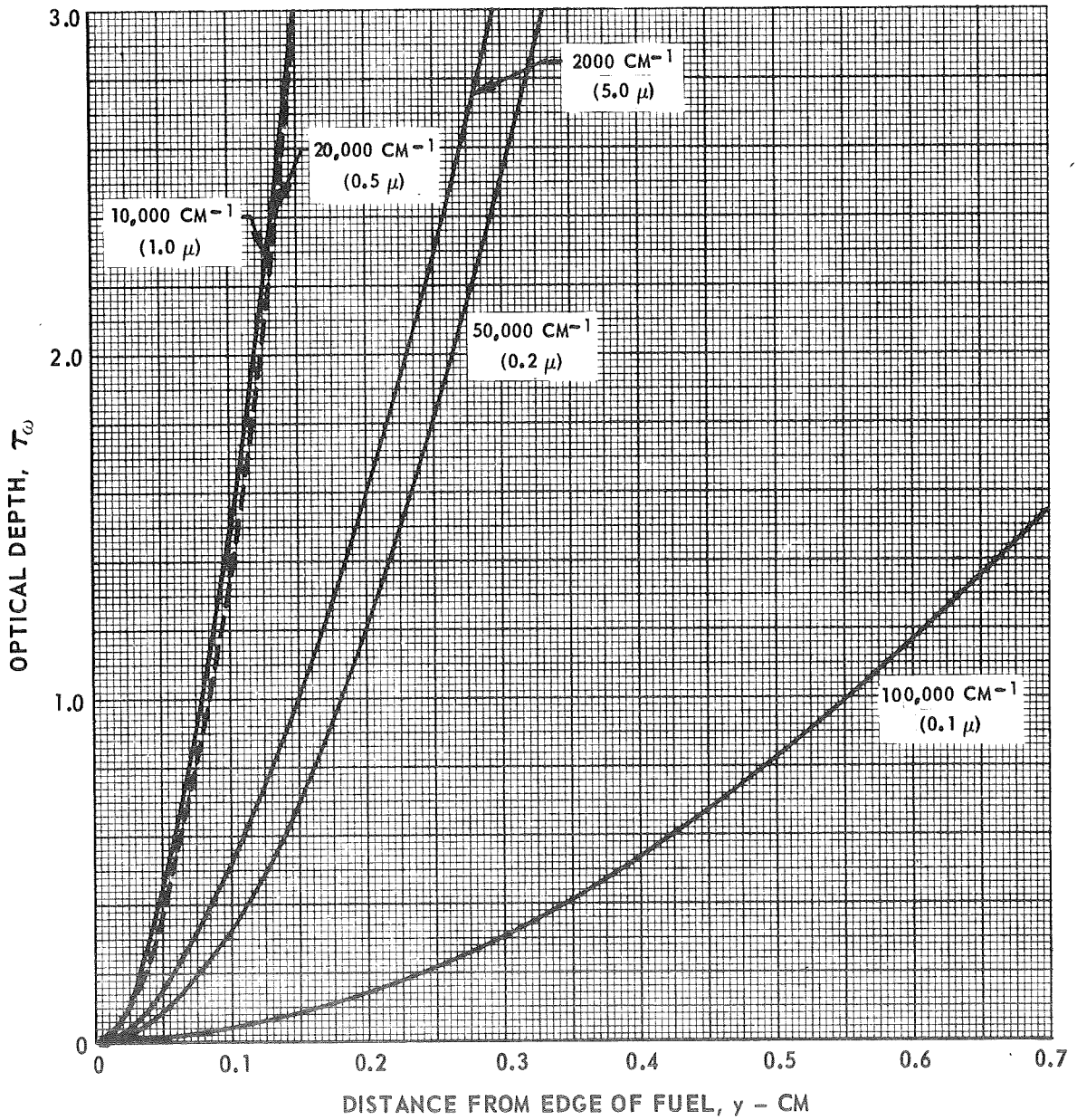

OPTICAL DEPTH DISTRIBUTION AT REPRESENTATIVE WAVE NUMBERS FOR CASE 6

$T^* = 15{,}000\ ^\circ R$
$Q^* = 24{,}300\ BTU/FT^2\text{-}SEC$

$$\tau_\omega = \int_0^y a_\omega\, dy$$

IP – LOW
MODEL – CONT
SEED – NONE
r_ω – ALUMINUM

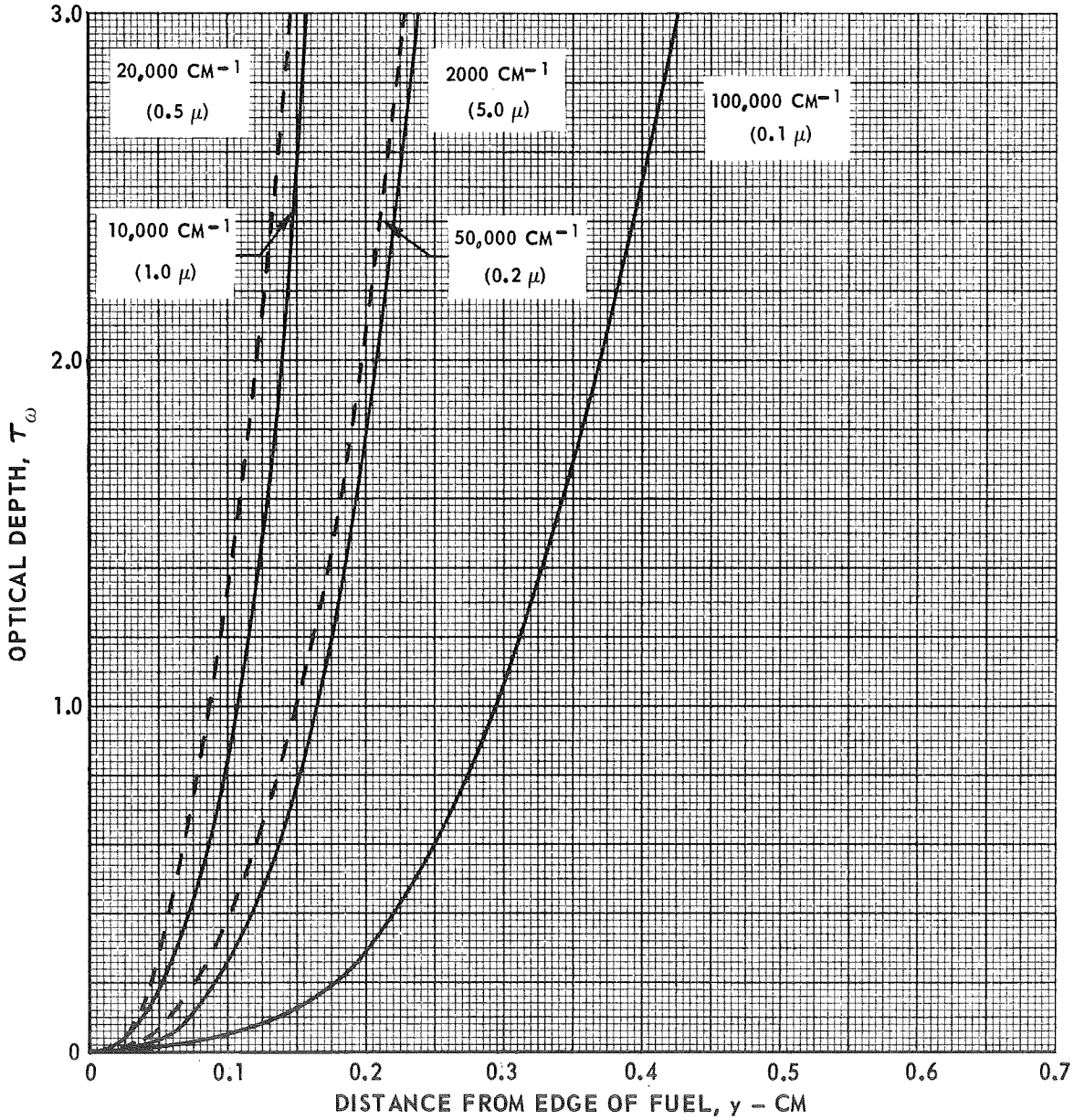

FIG. 28

BLACK BODY SPECTRAL FLUX AT REPRESENTATIVE WAVE NUMBERS AS A FUNCTION OF TEMPERATURE

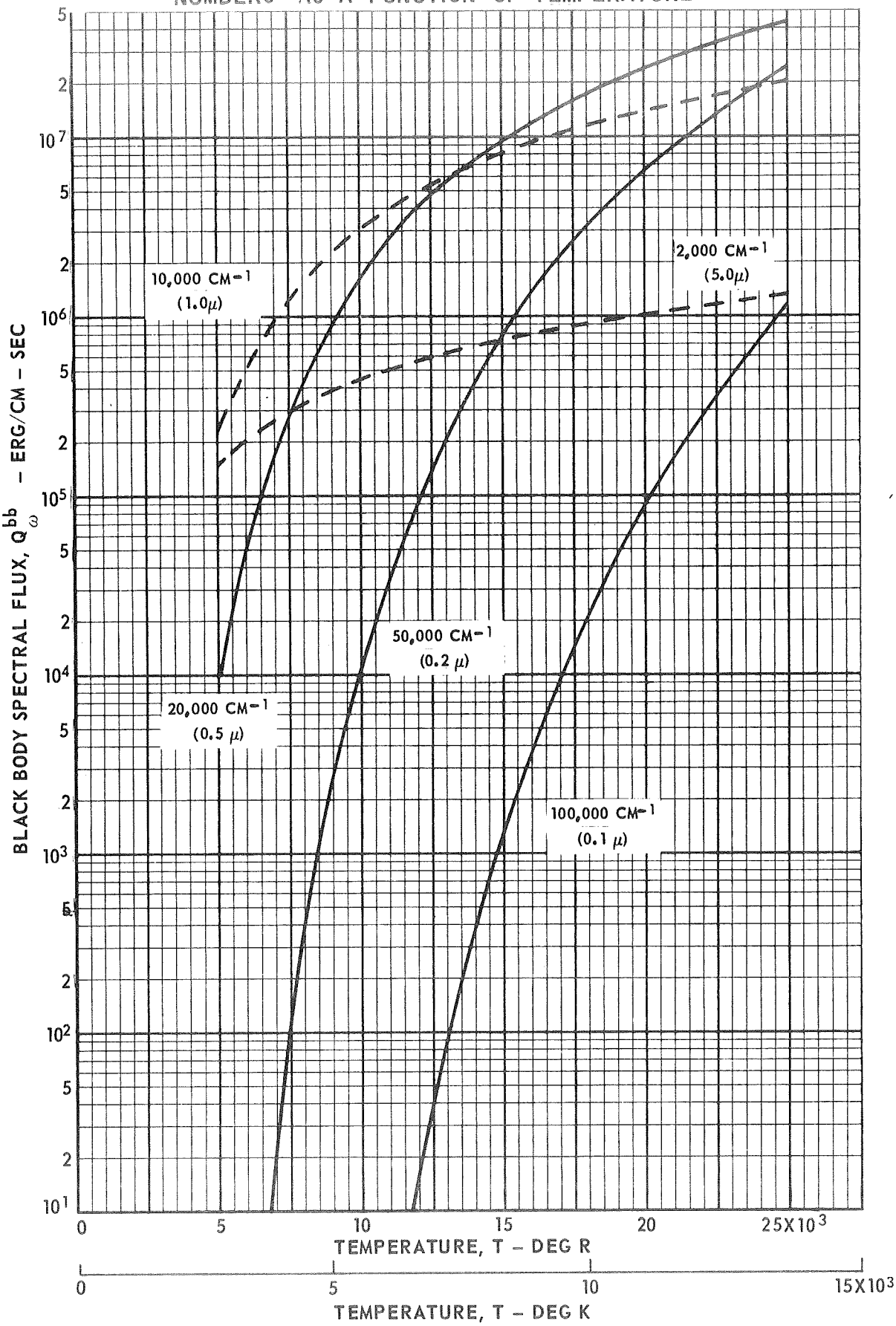

EFFECTIVE BLACK BODY RADIATING TEMPERATURE FOR ALL CASES AS A FUNCTION OF WAVE NUMBER

CASE	SYMBOL	IP	MODEL	SEED	r_ω
1	———	LOW	CONT	NONE	0
2	- - - - - -	HIGH	CONT	NONE	0
3	— - - —	LOW	BAND	NONE	0
4	— - - - - —	LOW	BAND	10.0 ATM HYDROGEN	0
5	— · —	LOW	CONT	NONE	UNIFORM
6	— · · —	LOW	CONT	NONE	ALUMINUM

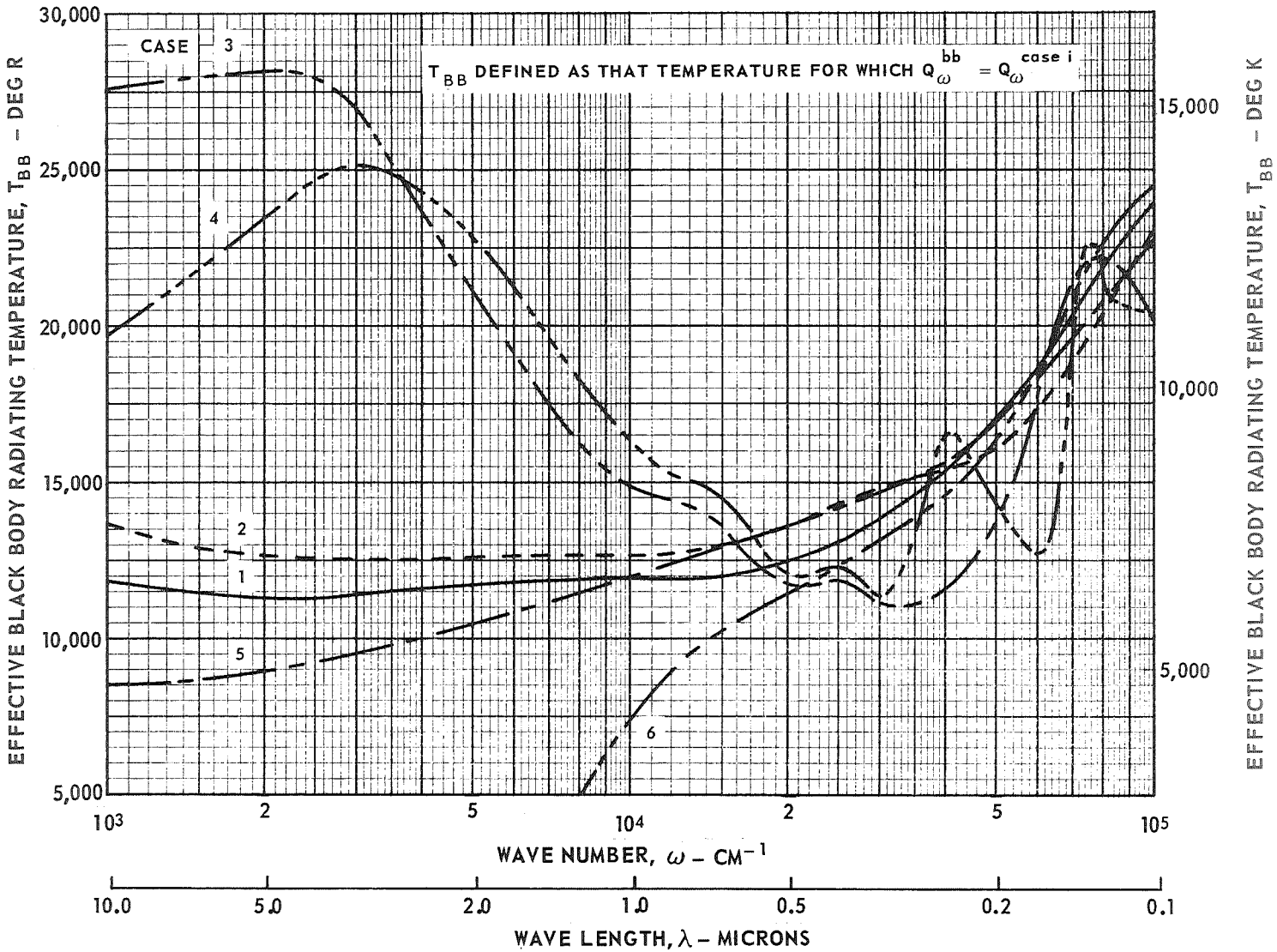

FIG. 29

EFFECT OPTICAL DEPTH FOR ALL CASES AS A FUNCTION OF WAVE NUMBER

CASE	SYMBOL	IP	MODEL	SEED	τ_ω
1	———	LOW	CONT	NONE	0
2	- - - -	HIGH	CONT	NONE	0
3	—·—·	LOW	BAND	NONE	0
4	—···—	LOW	BAND	1.0 ATM HYDROGEN	0
5	———	LOW	CONT	NONE	UNIFORM
6	SEE TEXT	LOW	CONT	NONE	ALUMINUM

$\tau_{\omega,E}$ DEFINED AS THE OPTICAL DEPTH AT WHICH T_{bb} EQUALS GAS TEMPERATURE

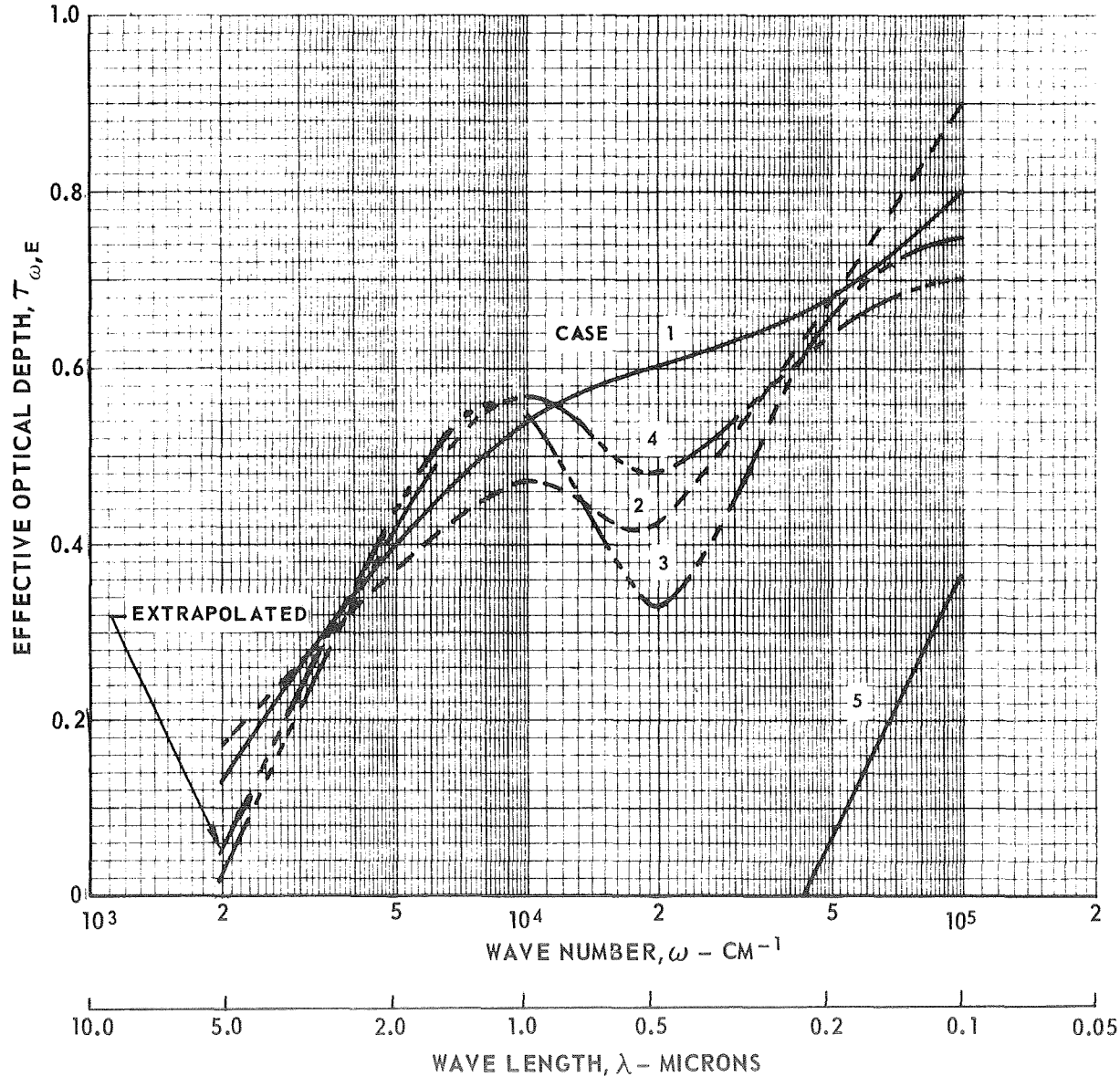

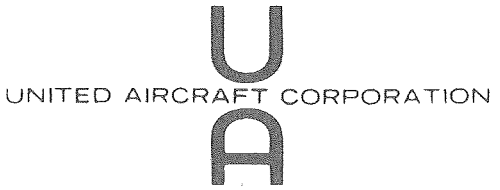
UNITED AIRCRAFT CORPORATION